NASA Contractor Report 4346, Part II

Effects of Engine Emissions From High-Speed Civil Transport Aircraft: A Two-Dimensional Modeling Study, Part II

Malcolm K. W. Ko, Debra K. Weisenstein,
Nein Dak Sze, Run-Lie Shia,
Jose M. Rodriguez, and Curtis Heisey

CONTRACT NAS1-18460
MARCH 1991

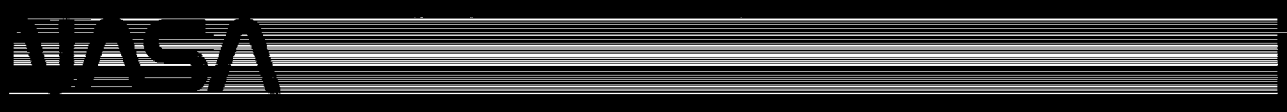

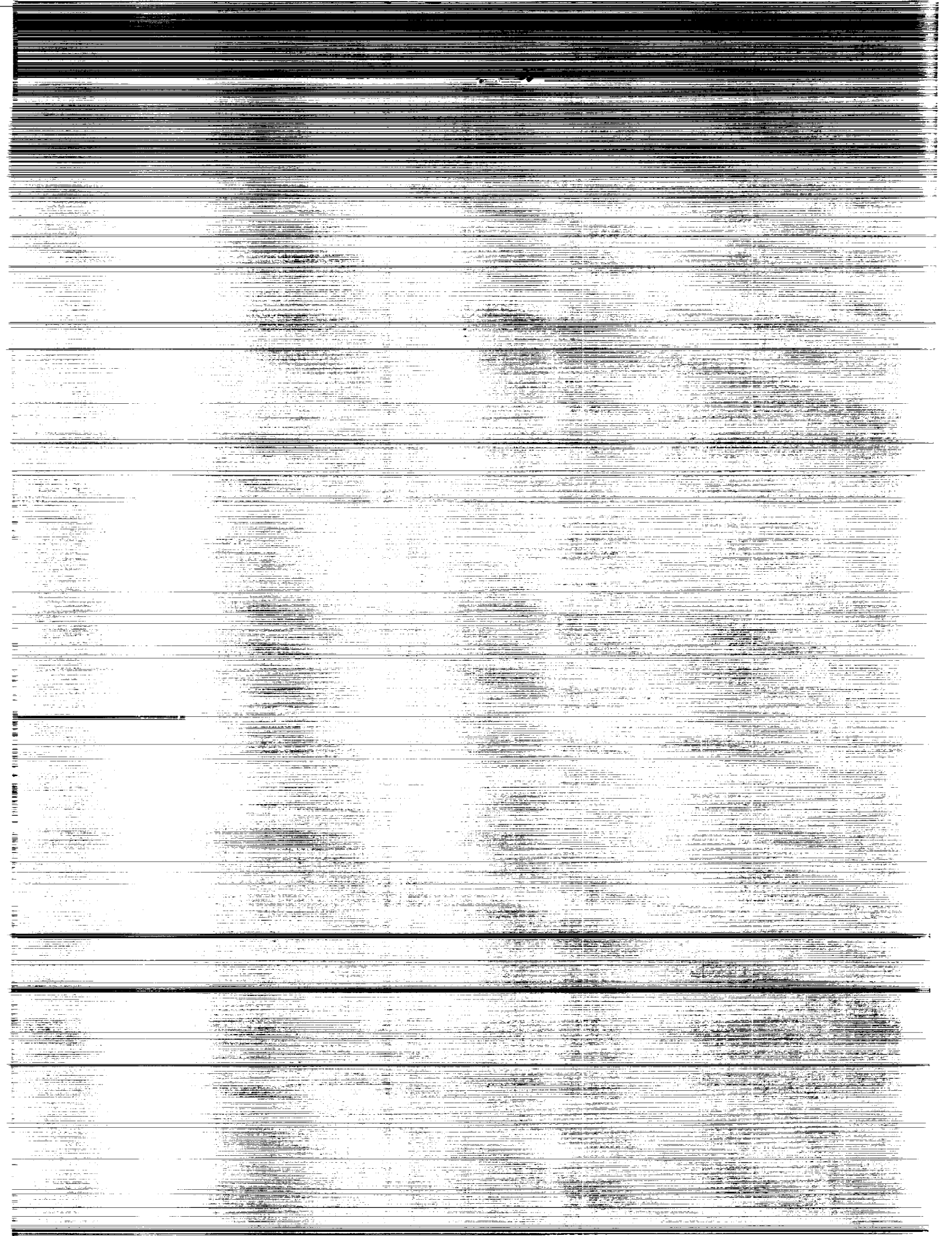

NASA Contractor Report 4346, Part II

Effects of Engine Emissions From High-Speed Civil Transport Aircraft: A Two-Dimensional Modeling Study, Part II

Malcolm K. W. Ko, Debra K. Weisenstein,
Nein Dak Sze, Run-Lie Shia,
Jose M. Rodriguez, and Curtis Heisey
Atmospheric and Environmental Research, Inc.
Cambridge, Massachusetts

Prepared by
Atmospheric and Environmental Research, Inc.
under Subcontract 89-6209-E2176
to ST Systems Corporation
for Langley Research Center
under Contract NAS1-18460

National Aeronautics and
Space Administration
Office of Management
Scientific and Technical
Information Division

1991

TABLE OF CONTENTS

Executive Summary

The AER two-dimensional chemistry-transport model is used to study the effect on stratospheric ozone (O_3) from operation of supersonic and subsonic aircraft in the 2010 atmosphere. Our results show that :

- the calculated O_3 response is smaller in the 2010 atmosphere compared to previous calculations performed in the 1980 atmosphere

- with the emissions provided to us, the calculated decrease in O_3 column is less than 1%

- the effect of model grid resolution on O_3 response is small provided that the physics is not modified.

I. Introduction and Summary

This is a continuation of our previous assessment study of the impact of emissions from High Speed Civil Transport (HSCT) aircraft on ozone (O_3). In our previous report, Ko et al (1989), we noted that the O_3 response is dominated by the portion of emitted nitrogen compounds that is entrained in the stratosphere and that the entrainment is a sensitive function of the altitude at which the material is injected. In addition, the O_3 removal efficiency of the emitted material depends on the concentrations of other trace gases in the background atmosphere. Consequently, evaluation of the impact of fleet operations in the future atmosphere must take into account the expected changes in trace gas concentrations from other activities.

Since the initiation of the work in the fall of 1987, we have been using the same version of the AER 2-D model for all of our assessment studies for reasons of continuity to facilitate direct comparison with previous results. In the interim, a number of improvements have been made to the AER 2-D model. This updated version of the model is used in the present study. The refinements include incorporation of bromine chemistry, refinement of the chlorine chemistry to include species such as Cl_2O_2 and OClO, parameterization of heterogeneous reactions and reassessment of the treatment of multiple scattering. For the purpose of the HSCT study, we also developed the coding to simulate the chemistry initiated by oxidation of C_2H_6 that leads to the formation of peroxyacetyl nitrate (PAN, $CH_3CO_3NO_2$). We consider this to be a first step in assessing the importance of longer chain hydrocarbons in the engine emissions. Other hydrocarbons can be treated in a similar manner using standard approaches in molecular-lumping technique (Lurmann et al, 1986) or structural-lumping technique (Gery et al, 1989).

We performed calculations on four (4) additional scenarios that were provided to us. These represent operation of a subsonic fleet and a supersonic fleet at Mach 2.4. The emissions differ from previous scenarios in the altitude distribution of the emitted materials and in the amount of nitrogen oxides emitted, reflecting changes in emission index. The calculations were performed relative to the 2010 background atmosphere. The calculated change in column abundance of O_3 in the case with the highest emission altitude was less than a 1% decrease in the northern polar region,

and about a 0.2% decrease in the southern polar region. The calculated O_3 column increase around 30°N is 0.4%. In another case, there is a small calculated increase for all latitudes and seasons.

With the calculated change in O_3 so small, the compensating effects from the O_3 increase in the troposphere due to operation of the subsonic fleet becomes more of an issue. We performed several simulations to separate the effects of the subsonic fleet and supersonic fleet by ascribing the effects from emissions below 40,000 ft to the subsonic fleet. Our calculations showed that emissions above 60,000 ft would decrease O_3 by about 0.1% at the tropics and up to 0.6% in the northern polar region. However, for emission between 40,000 ft and 55,000 ft, there is actually a calculated increase. The results point again to the importance of having a realistic treatment for the exchange process between the troposphere and stratosphere.

We performed some analyses as a first step in assessing the impact of the vertical resolution of the model grid on the model calculated O_3 results. A high-resolution (HR) version of the AER 2-D model was developed to solve for NOY concentrations and to assess the impact of emissions on the NOY concentration. The vertical resolution in the HR model is about 1.2 km compared to the 3.6 km spacing in the old model. We found that, with the type of emissions we are using, the coarse-resolution model underestimates the amount of NOY added to the stratosphere by up to 10% in the mid-stratosphere. In the region along the flight corridor, the calculated differences vary between 10-30%. We estimated the effect on the calculated O_3 to be small. It should be noted that the transport circulation for the HR model is obtained by interpolating the stream function from the old model. Thus there is no change in physics. The conclusion may not hold if we introduce new physics to describe the exchange process.

In section II, we will discuss the model enhancement and show how the results have changed compared to a case in the previous report. The response in the 2010 atmosphere will also be discussed and compared to the old results using a 1980 atmosphere. The results for the new emissions are presented in section III. The results from the high-resolution model are presented in section IV.

II. Model Enhancements

We have used the same version of the AER 2-D chemistry-transport model for the past 18 months since the HSCT study was initiated in the fall of 1987. In the mean time, a number of refinements have been made to the AER model through our on-going modeling efforts. These include adjustment of the water vapor concentration to account for in situ production from methane oxidation, and refinement of tropospheric washout for NOY and of the multiple scattering algorithm. The water vapor adjustment allows for an increase in the stratospheric concentration of H_2O due to oxidation of CH_4 (see e.g. Jones et al, 1986). Thus the projected increase in CH_4 in the year 2010 will also result in an increase in stratospheric H_2O.

A number of new species have been added to the chemical scheme. These include the hydrocarbon C_2H_6 along with full ethane chemistry leading to formation of PAN (see section C for discussion). The chemical scheme also includes bromine chemistry with CH_3Br and two industrial halons, H-1211 ($CBrC\ell F_2$) and H-1301 ($CBrF_3$), as the source gases. The chlorine chemistry scheme has been refined to include species such as $C\ell_2O_2$ and $OC\ell O$. The species F-22 ($CHC\ell F_2$) is added as a surrogate for the hydrogenated flurochlorocarbons. A simple parameterization for heterogeneous reactions is added to the scheme. However, none of the reactions are "turned on" for the present study.

A. Comparisons with Previous Results

The change in column O_3 due to HSCT emissions from scenario B7 calculated using the new version of the model will be presented to allow for comparison of previously modeled scenarios with the additional scenarios presented here. The ozone change due to B7 emissions from our previous report (Ko et al, 1989) is reproduced here as Figure 1(a) which shows the impact of aircraft emissions within the 1980 background atmosphere. When this scenario is reproduced with the updated version of the AER model, there is a 0.25% offset in the calculated O_3 column percent difference (i.e., the magnitude of the decrease was reduced by 0.25%). As shown in Figure 1(b) the equatorial ozone column showed no change due to B7 emissions, the high latitude northern hemisphere ozone column decreased by 1-2%, and the southern hemisphere ozone column decreased by 0.25-0.75%.

B. Results in 2010 Atmosphere Versus 1980 Atmosphere

The ozone response to aircraft emission scenarios B11 through B14 will be presented in the context of the 2010 background atmosphere, since HSCT aircraft could come into commercial operation in approximately 20 years. The 2010 atmosphere differs from the 1980 atmosphere used in our previous report in the concentrations of N_2O, CH_4, and total odd chlorine. See table 1 for a list of boundary conditions used in the 1980 and 2010 background atmospheres. The N_2O concentration increased by 9%, the CH_4 by 23%, and the total odd chlorine increased from 2.57 ppb to 4.70 ppb, or 83%. Calculated total ozone column amounts are 2-5% lower in the 2010 background atmosphere than in the 1980 atmosphere.

The ozone column as a function of latitude and season calculated by the model for the 2010 baseline atmosphere is shown in figure 2. Latitude by height cross-sections of ozone mixing ratio for January, April, July and October are shown in figure 3. Concentrations of total odd nitrogen (NOY) are shown in figure 4. Figures 5 and 6 show concentrations of CO and CH_4, respectively. Figure 7 shows the water vapor concentration, which does not vary by season. Figures 8 and 9 show concentrations of C_2H_6 and PAN, species not included in previous model calculations of HSCT impacts, but which may be important.

In the previous study of the impact of HSCT emissions on ozone (Ko et al, 1989), we found that increasing N_2O makes the ozone more sensitive to HSCT emissions so that the calculated O_3 decrease is larger.. Increasing CH_4 decreases the sensitivity of ozone to HSCT emissions. Increasing total odd chlorine also decreases the sensitivity. Based on the relative changes in N_2O, CH_4, and odd chlorine, we would expect HSCT emissions to cause less ozone depletion in 2010 than in 1980. Figure 10 shows the impact of B7 emissions on ozone column within the 2010 background atmosphere. Note that B7 HSCT emissions produce an O_3 increase from 30°S to 40°N within the 2010 atmosphere. Maximum depletion of 1.2% occurred at the north pole in spring.

C. PAN Chemistry

The species $CH_3CO_3NO_2$ (PAN) is one of the products of the oxidation of ethane (C_2H_6) and other non-methane hydrocarbons. The oxidation chain is started by the reaction:

$$C_2H_6 + OH. \rightarrow C_2H_5 + H_2O \quad (1)$$

followed by rapid formation of $C_2H_5O_2$ through the reaction

$$C_2H_5 + O_2 \ (+M) \rightarrow C_2H_5O_2 \ (+M). \quad (2)$$

Further oxidation of $C_2H_5O_2$ results in formation of acetaldehyde (CH_3CHO) through the reaction

$$C_2H_5O_2 + NO \rightarrow CH_3CHO + NO_2 + HO_2 \quad (3)$$

and through the chain of reactions

$$C_2H_5O_2 + HO_2 \rightarrow C_2H_5OOH + O_2, \quad (4)$$

$$C_2H_5OOH + h\nu \ (+O_2) \rightarrow CH_3CHO + HO_2 + OH. \quad (5)$$

Oxidation of acetaldehyde in turn leads to production of CH_3CO_3 through

$$CH_3CHO + OH \ (+O_2) \rightarrow CH_3CO_3 + H_2O. \quad (6)$$

Peroxyacetyl nitrate is then formed by the reaction

$$CH_3CO_3 + NO_2 \ (+ M) \rightarrow CH_3CO_3NO_2 \ (PAN) \quad (7)$$

and removed by thermal decomposition

$$CH_3CO_3NO_2 + M \rightarrow CH_3CO_3 + NO_2 \quad (8)$$

and photolysis

$$CH_3CO_3NO_2 + h\nu \rightarrow \text{products}. \quad (9)$$

We have modified our photochemical module in the 2-D model to include the reactions important in the formation and removal of PAN. In particular, we have also included in our photochemical module a complete scheme for ethane

oxidation. This scheme is similar to the one described by Kasting and Singh (1986). Kinetic data has been taken from the latest review by Atkinson et al. (1989). Unknown rates for reactions in the oxidation chain of ethane have been assumed the same as the rates of similar reactions in the oxidation chain of methane. We have included PAN as an additional species in the NOY family.

Reported rates for the thermal decomposition of PAN are very sensitive to temperature. As the tropospheric temperature decreases with altitude, the thermal decomposition rate decreases dramatically. Removal time constants by both photolysis and thermal decomposition are of order 10^7 seconds above 5 km. As a result, the calculated concentration of PAN increases with altitude in the troposphere, and becomes an important NOY species in the upper troposphere and lower stratosphere with the PAN abundances comparable to those of NO_2.

There are still considerable uncertainties in the present kinetic data for reactions in the oxidation chain of ethane and for the formation and decomposition of PAN. In particular, we note the following uncertainties:

- The formation rate of PAN (reaction 8) has been measured at both low pressures (76-612 Torr) and at high pressures (1 atm; see review by Atkinson et al., 1989). However, all these measurements have been carried out at room temperature (298°K). The pressure dependence has been obtained by adopting the standard Troe formula for three-body reactions. Since the temperature in the region where PAN is important (5-10 km) ranges from about 240 to 220°K, it is imperative to obtain kinetic data at these temperatures. Given the behavior of other three-body reactions, we expect the formation rate to increase with decreasing temperature. It is also important to conduct further studies of the pressure dependence of this rate.

- The temperature dependence for the thermal decomposition rate has been determined from data in a temperature range of approximately 295 - 320°K (Atkinson et al., 1989). Thermal decomposition rates are extremely sensitive to temperature, and we may expect large uncertainties because the recommended values are used at temperatures typical of the upper troposphere - lower stratosphere. Further measurements are needed for temperatures and pressures appropriate to these regions.

Given the considerable uncertainties in the present kinetic data, it is conceivable that PAN could be a major NOY species also in the stratosphere. Developments in the study of these reactions should be included in future detailed assessments of the possible impact of PAN in the chemistry of HSCT exhaust gases.

We performed a calculation to determine the effect of treating the hydrocarbon emissions in scenario B7 as emissions of C_2H_6 rather than CH_4. Because C_2H_6 contains two carbon atoms, the number of molecules per second emitted as C_2H_6 was half of the CH_4 emissions. Increasing the C_2H_6 through HSCT emissions increased PAN concentrations only in localized areas: at 20 km and 30°N to 70°N and during summer and fall at 50°N and 6 km. Only the low altitude PAN increase in summer and fall had an impact on O_3, and because of its low altitude, made a negligible difference in ozone column.

III. Results for Scenarios B11-B14

A. Emissions

The emission scenarios presented here, designated B11, B12, B13, and B14 were provided by the Boeing Corporation and are similar in emission altitudes to scenario B7 in our previous report. They include emissions of nitrogen oxides (NO_x), carbon monoxide (CO), hydrocarbons, sulfur dioxide (SO_2), carbon dioxide (CO_2), and water vapor from both subsonic and supersonic aircraft fleets. As in our previous report, we did not include SO_2 and CO_2 emissions in the model calculations. Water vapor concentrations were increased based on water vapor emissions and the change in the model's CH_4 concentration, but were not transported within the model. Nitrogen oxide emissions were input to the model as NOY, or total odd nitrogen.

Emissions were provided at three height levels, 26000 ft, 37000 ft, and an additional level which varied from 50000 ft to 65000 ft. Table 2 shows the emissions of NOY, CO, CH_4, and H_2O at each height level for scenarios B7, B11, B12, B13, and B14. Emissions at the lower two levels are similar to those levels in scenario B7, but the upper level NOY emissions are 1/2 to 2/3 of the B7 emissions at the upper level, reflecting a different emission index (EI). Scenarios B11-B14 all represent HSCT aircraft using the same engine but with different cruise altitudes. Notice that the scenarios which have a higher cruise altitude for the HSCT aircraft have somewhat lower emissions.

The latitudinal distribution of emissions for the 4 scenarios is shown in figures 11-14 for NOY, CO, CH_4, and H_2O, as interpolated onto the AER model's latitude grid. Ninety percent of the NOY emissions occur in the northern hemisphere, and 60% of the emissions occur between 30°N and 60°N for the highest emission altitude of each scenario. This means that the majority of the ozone impact occurring in the southern hemisphere is due to inter-hemispheric transport from the northern mid-latitudes.

In our previous report, we concluded that the ozone response was proportional to the amount of NOY entrained in the stratosphere, which is very sensitive to the altitude of injection of emissions. Scenarios B11-B14 differ in their altitudes of stratospheric emission as well as the magnitude of emissions. The AER 2D chemical-transport model has a vertical resolution of 3.6 km. Using this model, the emissions from scenarios B11 and B14 are put

into the same model grid levels. The same holds true for B12 and B13. Because the NOY emissions for scenarios B11 and B14 are at the same model grid levels and differ in magnitude by only 3%, model results from these two scenarios are almost identical. By modeling the NOY emissions from these two scenarios within a high-resolution model, we conclude that our chemistry-transport model represents the emissions of B14 better than B11. Therefore we will show results from scenario B14 here, but will present results from both scenarios B11 and B14 in Section IV.

Scenario B13 has 16% greater NOY emissions between 50000 and 55000 ft than does B12. However, the emissions for B12 are put into a higher altitude. When modeled within the AER chemistry-transport model where the emission are put into the same model grid level, scenario B13 had the greater NOY entrainment. However, the opposite could be the case if the difference in emission altitudes were resolved. In this section, we will present results only from scenario B12, which produced NOY results that more closely match the results from the high-resolution model. Results from the high-resolution model for both scenarios B12 and B13 will be shown in Section IV.

B: O_3 Response to Engine Emissions

The response of ozone to emission of NOY, CO, CH_4, and H_2O from aircraft engines will be presented in the context of the projected background atmosphere in the year 2010. As we found in our previous report, we again expect the majority of the ozone impact to be due to the NOY emissions.

Scenario B14 had emissions at 26000 ft, 37000 ft, and 65000 ft, corresponding to model altitude levels 3 (8-12 km), 4 (12-14 km), and 6 (18-22 km). The change in NOY concentration in ppb produced by this scenario is shown in figure 15. The NOY increase is as much as 0.3 ppb in the southern hemisphere and up to 0.5 ppb at the equator. Because emissions occur at a height well within the stratosphere, there is efficient global dispersal. The maximum local change, occurring at 12-14 km and 40-60°N, is 2-3 ppb.

The change in CO concentration due to emissions from scenario B14 is shown in figure 16. CO increased only between 10 and 20 km, the region in which emissions occurred. In other regions of the model atmosphere, it was more strongly influenced by changes in OH due to water vapor emissions. CH_4 also responded to the change in OH and decreased everywhere throughout the

model atmosphere within scenario B14. Figure 17 shows the CH_4, which decreased by as much as 12 ppb in the middle stratosphere. The change in H_2O vapor concentration is shown in Figure 18. H_2O increased by 0.3-0.4 ppm throughout most of the stratosphere, producing an OH increase of 2-4%.

The change in O_3 mixing ratio as a percentage of the 2010 baseline for scenario B14 is shown in figure 19. Compared to the B7 O_3 impact from our previous report, the area of O_3 increased is enlarged, with O_3 increases up to 15 km in both hemispheres. This is substantially due to the difference in multiple scattering treatment in the lower atmosphere. Ozone increases of 8-12% are found in the northern hemisphere at 8-10 km. Ozone decreased by 1-2% over most of the middle stratosphere. The influence of transport is seen in the fact that ozone decreases of 2-4% are seen only in spring at 15 km near the north pole. The circulation is downward at northern high latitudes in winter and spring, tending to concentrate the emitted odd nitrogen and increase its impact on ozone.

The percent change in ozone column from the baseline atmosphere due to emissions of NOY, CO, CH_4, and H_2O for scenario B14 is shown in figure 20. The ozone column has increased year-round at equatorial latitudes and at northern latitudes in late summer and fall. Ozone increased by 0.4 to 0.6% at 30°N. This latitude corresponds to the boundary between the high equatorial tropopause and the lower mid-latitude tropopause assumed in the model. Emissions in this region were large enough to increase tropospheric ozone by 4-8%. The northern hemisphere ozone column decrease, with maximum value of 0.8%, is centered at the north pole in April, where the ozone column maximum is also located. Southern hemisphere ozone decreased by 0.1 to 0.3%.

The change in NOY from the baseline in ppbv for scenario B12 is shown in figure 21. The maximum change is 2 ppbv. The global change is less than 0.1 ppbv above 40 km. With emissions at a height of 55000 ft in scenario B12, there is substantially less NOY entrained in the stratosphere than with scenario B14 which has emissions at 65000 ft. The changes in CO, CH_4, and H_2O for scenario B12 are shown in figures 22, 23, and 24, respectively. Because of the height of emissions, very little H_2O vapor from the aircraft engines was entrained in the stratosphere, and therefore CO and CH_4 show a much smaller OH effect, ie. less of a decrease. CH_4 shows an increase in concentration from 10 to 20 km.

The change in local ozone mixing ratio, as a percentage of the baseline, is shown in figure 25. Due to the altitude of emissions, there is very little ozone depletion except in spring near the north pole. The ozone column change, shown in figure 26, is positive everywhere except near the north pole in spring. There was an increase in column O_3 of up to 1% at 40°N.

C. Impact of Supersonic Versus Subsonic Emissions

In order to separate the effects of the stratospheric emissions at 65000 ft which are due entirely to HSCT aircraft and emissions below 40000 ft which are due substantially to fleets of subsonic aircraft, we have repeated the model calculations using B14 emissions at 65000 ft only and B14 emissions at the two lower levels, 26000 ft and 37000 ft. The change in O_3 column due to low level emissions for this scenario is shown in figure 27(a). The ozone column increased everywhere with a seasonal pattern similar to that of the full B14 scenario. Figure 27(b) shows the ozone column change for scenario B14 emissions at 65000 ft only. The ozone column decreased from 0.1% to 0.6%. Figure 28 shows the change in ozone column from scenario B14 with emissions at all levels as a percentage of the ozone column with scenario B14 emissions at the lower levels only. This represents the expected change in the 2010 atmosphere with HSCT aircraft and subsonic aircraft compared with an atmosphere with only subsonic aircraft. The ozone column change varies from -0.1% to -0.8%.

The change in column O_3 due to B12 emissions at the lower two levels only is shown in figure 29(a). This figure is the same as figure 27(a), since emissions at the lower two levels were almost identical for all four scenarios. The O_3 column change due to emissions at the 55000 ft level only is show in figure 29(b). Compared to the baseline atmosphere, these emissions produced an O_3 increase of 0.1-0.3% in the northern hemisphere and had little impact in the southern hemisphere. Emissions at 55000 ft are efficiently transported into the troposphere where they enhance O_3 concentrations. Figure 30 show the change in O_3 column for the case with B12 emissions at all levels compared with the low level emissions only, again to represent the impact of HSCT emissions in an atmosphere with subsonic aircraft. Ozone column changes are both positive and negative but very small, varying from -0.175 to +0.05%.

If a large fleet of HSCT aircraft were to be put into service, we would expect that these supersonic aircraft flights would replace a portion of the subsonic flights as people who would travel anyway opt for faster transport. There may be some increase in the number of travelers as quicker trans-Pacific travel makes such journeys more attractive. If the major impact on airline travel proves to be a shift from subsonic to supersonic travel, then the relative impact of HSCT's will be somewhat greater as the low level emissions which produce O_3 will be reduced.

In our previous report, we concluded that emissions below 18 km had only a small impact on the ozone column. However, the emission scenarios studied in that report had at least twice the upper level emissions of the scenarios studied here, and this changes the relative importance of high and low level emissions. Comparing figure 20 and figure 27(b), we see that emissions at the 65000 ft level only produce an ozone column decrease at all latitudes while emissions at all three levels produce an ozone column increase from 30°S to 50°N.

IV. High Resolution Model Results

A. Model Description and Analysis

A high-resolution version of the AER two-dimensional model with simplified chemistry was developed to study the effects on stratospheric NOY from high speed civil transport aircraft (HSCT) operation. The use of the model with finer vertical resolution is necessary for investigating the sensitivity of the amount of NOY retained in the stratosphere to emission altitude, height of tropopause and exchange between the troposphere and stratosphere. The higher resolution is necessary to resolve the difference between scenarios B11 and B14 and between scenarios B12 and B13.

The vertical resolution of the model was increased by a factor of three, i.e. every horizontal layer in the original grid was equally divided into 3 layers in Z coordinates, where

$$Z = H \log \left(\frac{P_s}{p}\right) \tag{10}$$

The horizontal resolution was unchanged. The seasonally-varying temperature, pressure, streamfunction, and eddy diffusion coefficients were interpolated to the new grid. There was no attempt to improve the model physics to better represent physical processes within the finer resolution model.

This model was used to solve for NOY only, using seasonally-varying production and loss rates from a previous run of the chemical-transport model which was interpolated onto the fine-resolution grid. The NOY concentration responds only to transport, to the input production and loss rates, and to HSCT emissions. Because NOY chemistry involves only production through the reaction $N_2O + O(^1D)$, washout in the troposphere, and quadratic loss at high altitude, its response to HSCT emissions should be independent of other species to first order. And because ozone change due to HSCT emissions is roughly proportional to the increase in NOY, we can use these results to estimate the impact of emissions on ozone.

Two kinds of emission scenarios were examined in this study: scenario B8 from our previous study and scenarios B11, B12, B13, B14, which had emissions at 3 discrete altitude levels, and scenario A4 from our previous study which had emissions that were continuous with altitude up to 24 km. Scenario A4 was previously provided by the McDonnell-Douglas Corporation. See table 3 for NOY emissions associated with scenarios B8 and A4.

1. Impact of model resolution

In order to compare results from the fine-resolution model and the coarse-resolution model, scenario B8 was run with the fine resolution-model and also with a coarse-resolution version of the same model. In order to compare results, the fine-resolution results were degraded into the coarse-resolution grid using a scheme which preserves mass within grid boxes. Figure 31 shows the difference between the fine- and coarse-resolution models in percent for the clean atmosphere without HSCT emissions. The fine-resolution model shows larger mixing ratios by 0-2% over most of the stratosphere, with larger increases of up to 30% in the mid and high latitude lower stratosphere. In the tropical troposphere, the fine-resolution model shows smaller mixing ratios by 5-30%. Figure 32 shows differences in NOY column abundance as a function of latitude and season for the same clean atmosphere case. Differences between fine- and coarse-resolution models are -3% at the equator, 5% at northern high latitudes, and 4-7% at southern high latitudes.

For the HSCT study, the quantity of interest is the difference between NOY concentrations with and without emissions. Figure 33 shows the difference in percent between the high-resolution change in NOY and the coarse-resolution change in NOY with and without emissions. The plotted quantity is:

$$([B8 - base]_{HR} - [B8\text{-}base]_{LR}) / [B8\text{-}base]_{HR} \times 100 \qquad (11)$$

where [B8-base] represents the calculated change in NOY due to the engine emissions and the subscripts HR and LR denote quantities calculated using the high-resolution and coarse-resolution models, respectively. The coarse-resolution model underestimates the entrained NOY by about 10% in a broad region of the stratosphere above 30km. The amount entrained below 30 km is underestimated by as much as 30% except for two narrow bands between 15-20 km and 10-15 km when the value is less than 10%. There are small areas of negative values in figures 33 corresponding to overestimation by the coarse-resolution model. These are found around the tropopause, at regions when there are large injections and near the winter pole in the upper stratosphere. It is likely that these are due to the numerical noise in the model treatments. Column differences with B8 emissions versus no emissions, shown in figure 34, are calculated in a similar manner as defined in (11). The figure shows that the coarse-resolution model underestimates the NOY entrainment by about 0-6%.

2. Sensitivity to tropopause height and injection altitude

We ran 3 test cases for the A4 scenario, in which the tropopause was moved up 1 and 2 layers and down 1 layer respectively within the fine-resolution model. It is clear from figure 35 that the response of the change of NOY column abundance to the change of tropopause is almost linear because of the continuity of the sources in the A4 scenario.

To study the sensitivity of the NOY increase to the emission altitude within the fine-resolution model, we used the B8 scenario with the top level of emissions only. This source, which was normally put into the 17th altitude level, was put into 4 successively lower levels (levels 16-13). From figure 36, a sudden decrease in the column abundance can be seen when the source was moved from the 15th to the 14th layer, where the tropical tropopause is located.

The model results for NOY increase are very sensitive to the position of the tropopause and emission altitude, especially for scenarios with discontinuous emission altitudes. If more accurate results are desired, there is a need to adjust the tropopause and input data to find a better calibrated fine-resolution model. This could be achieved by performing model simulations and using nuclear debris data for validation (see e.g. Shia et al, 1989).

B. NOY Results for Scenarios B11-B14

NOY results from the fine resolution model for scenarios B14, B11, B12, and B13 are shown in figures 37-40, respectively. The NOY change for scenario B14 with the fine resolution model is very similar to that obtained with the coarse-resolution chemistry-transport model (comparing figure 15 with figure 37) at high altitudes and in the southern hemisphere, which indicates similar stratospheric entrainment and transport. Comparing the fine-resolution model results for B12, shown in figure 39, with figure 21 shows that the fine-resolution model retained more NOY from a source at 55000 ft than did the chemistry-transport model.

There is very little difference between the results from B14 and B11 (figures 37 and 38), which differ only by 5000 ft in emission altitude at the top level. This indicates little difference in stratospheric entrainment between emissions at 65000 ft and emissions at 60000 ft since both are well

above the tropopause. However, when the height of emissions drops from 60000 ft to 55000 ft (compare figures 38 and 39, scenarios B11 and B12), then the stratospheric NOY increase drops from 0.3 ppbv to 0.2 ppbv despite the 10% increase in emission magnitude at the upper level. And when the emission altitude drops to 50000 ft (see figure 40, scenario B13), the stratospheric NOY increase drops to less than 0.1 ppbv. Because of its higher altitude of emissions, scenario B12 shows greater entrainment of NOY in the stratosphere, even though B13 has 16% greater emissions at the 50,000-55,000 ft level.

C. Estimates of Ozone Impacts

By degrading the NOY concentrations obtained with the high-resolution model for use in the coarse-resolution chemistry-transport model, we can obtain estimates for ozone impacts for scenarios B11-B14. We do this by reading the seasonally-varying NOY concentration into the model rather calculating it. With this mode of operation, NOY impacts O_3 and other species within the model but does not respond to changes in O_3, i.e. there is no chemical feedback between NOY and other species. However, the odd nitrogen species (NO, NO_2, HNO_3, PAN, etc.) are partitioned based on model-calculated O_3, OH, $O(^1D)$, and other species.

Scenarios B14 and B11 would yield almost identical O_3 changes, since their NOY responses are very similar. Scenarios B12 and B13 have emissions near the tropopause, in the region which is sensitive to stratospheric entrainment. Figures 41(a) and 42(b) show calculated ozone impacts from scenarios B12 and B13, respectively, using high-resolution NOY within the coarse-resolution model. The difference in calculated O_3 impact between scenarios B12 and B13 is small.

References

Atkinson, R., D. L. Baulch, R. A. Cox, R. F. Hampson, J. A. Kerr, and J. Troe (1989) Evaluated kinetic and photochemical data for atmospheric chemistry: Supplement III. J. Phys. Chem. Ref. Dat., 18, 881-1097.

Gery, M.W., G.Z. Whitten, J.P. Killus, and M.C. Dodge (1989) A photochemical kinetics mechanism for urban and regional scale computer modeling. J. Geophys. Res., 94, 12,925-12,956.

Jones, R.L., J.A. Pyle, J.E. Harries, A.M. Zavody, J.M. Russell III, J.C. Gille (1986) The water vapor budget of the stratosphere studied using LIMS and SAMS satellite data. Quart. J. R. Met. Soc., 112, 1127-1143.

Kasting, J. F., and H. B. Singh (1986) Non-methane hydrocarbons in the troposphere: Impact on the odd hydrogen and odd nitrogen chemistry. J. Geophys. Res., 91, 13,239-13,256.

Ko, M.K.W., D.K. Weisenstein, N.D. Sze, J.M. Rodriguez, C. Heisey (1989) Effects of Engine Emissions from High Speed Civil Transport Aircraft: A two-dimensional modeling study. Final Report 88-6209-D1417, prepared for ST Systems Corporation by Atmospheric and Environmental Research, Inc., 840 Memorial Drive, Cambridge, MA.

F.W. Lurmann, A.C. Lloyd and R. Atkinson (1986) A chemical mechanism for use in long-range transport/acid deposition computer modeling. J. Geophys. Res., 91, 10905-10936.

NASA/JPL (1988) Chemical Kinetics and Photochemical Data for Use in Stratospheric Modeling. Evaluation Number 8. JPL Publication 87-41.

Remsberg, E.E., J.M. Russell, III, L.L. Gordley, J.C. Gille, and P.L. Bailey (1984) Implications of the stratospheric water vapor distribution as determined by the Nimbus 7 LIMS experiment. J. Atmos. Sci., 41, 2934-2945.

Shia, R.-L., Y.L. Yung, M. Allen, R.W. Zurek, and D. Crisp (1990) Sensitivity study of advection and diffusion coefficients in a two-dimensional stratospheric model using excess carbon 14 data. Accepted to J. Geophys. Res.

Table 1. Comparison of boundary conditions between this work and results in Ko et al (1989)

specie	Ko et al (1989) (1980 atmosphere)	This work (2010 atmosphere)
N_2O	300 ppb	325.7 ppb
CH_4	1.6 ppm	1.975 ppm
C_2H_6	*	1.8 ppb
CO	100 ppb	100 ppb
CH_3Cl	700 ppt	700 ppt
CCl_4	100 ppt	125 ppt
$CFCl_3$ (F-11)	170 ppt	368 ppt
CF_2Cl_2 (F-12)	285 ppt	671 ppt
CH_3CCl_3	100 ppt	230 ppt
$CHClF_2$ (F-22)	*	419 ppt
$C_2Cl_3F_3$ (F-113)	*	98.7 ppt
$CBrClF_2$ (H-1211)	*	1.71 ppt
$CBrF_3$ (H-1301)	*	6.6 ppt
CH_3Br	*	10 ppt

*Specie not included in the Ko et al (1989) model calculations.

Table 2. Emissions for Scenarios B7, B11, B12, B13, B14

NOY EMISSIONS (molecules/sec)

ft	B7	B11	B12	B13	B14
26000	1.36×10^{26}	1.36×10^{26}	1.36×10^{26}	1.36×10^{26}	1.36×10^{26}
37000	1.10×10^{27}	1.12×10^{27}	1.12×10^{27}	1.12×10^{27}	1.12×10^{27}
50000				1.34×10^{26}	
55000			1.16×10^{26}		
60000	1.99×10^{26}	1.05×10^{26}			
65000					1.02×10^{26}

CO EMISSIONS (molecules/sec)

ft	B7	B11	B12	B13	B14
26000	1.29×10^{25}	1.29×10^{25}	1.29×10^{25}	1.29×10^{25}	1.29×10^{25}
37000	4.02×10^{26}	1.19×10^{26}	1.19×10^{26}	1.20×10^{26}	1.19×10^{26}
50000				1.04×10^{26}	
55000			9.06×10^{25}		
60000	1.35×10^{26}	8.17×10^{25}			
65000					7.95×10^{25}

CH_4 EMISSIONS (molecules/sec)

ft	B7	B11	B12	B13	B14
26000	4.60×10^{24}	4.60×10^{24}	4.60×10^{24}	4.60×10^{24}	4.60×10^{24}
37000	8.58×10^{25}	4.38×10^{25}	4.40×10^{25}	4.43×10^{25}	4.37×10^{25}
50000				4.56×10^{25}	
55000			3.95×10^{25}		
60000	2.35×10^{25}	3.57×10^{25}			
65000					3.47×10^{25}

H_2O EMISSIONS (molecules/sec)

ft	B7	B11	B12	B13	B14
26000	2.13×10^{28}	2.13×10^{28}	2.13×10^{28}	2.13×10^{28}	2.13×10^{28}
37000	1.93×10^{29}	1.90×10^{29}	1.91×10^{29}	1.92×10^{29}	1.90×10^{29}
50000				1.00×10^{29}	
55000			8.68×10^{28}		
60000	8.62×10^{28}	7.83×10^{28}			
65000					7.62×10^{28}

Table 3. NOY Emissions for Scenarios B8, A4

B8 NOY EMISSIONS

ht (ft)	Emissions (molecules/sec)
26,000	1.36×10^{26}
37,000	1.13×10^{27}
58,500	4.05×10^{26}

A4 NOY EMISSIONS

ht (km)	Emissions (molecules/sec)
0-2	1.76×10^{25}
2-4	4.19×10^{24}
4-6	4.19×10^{24}
6-8	4.19×10^{24}
8-10	4.19×10^{24}
10-12	5.93×10^{24}
12-14	5.93×10^{24}
14-16	3.33×10^{24}
16-18	2.82×10^{24}
18-20	2.82×10^{24}
20-22	4.63×10^{25}
22-24	1.26×10^{26}

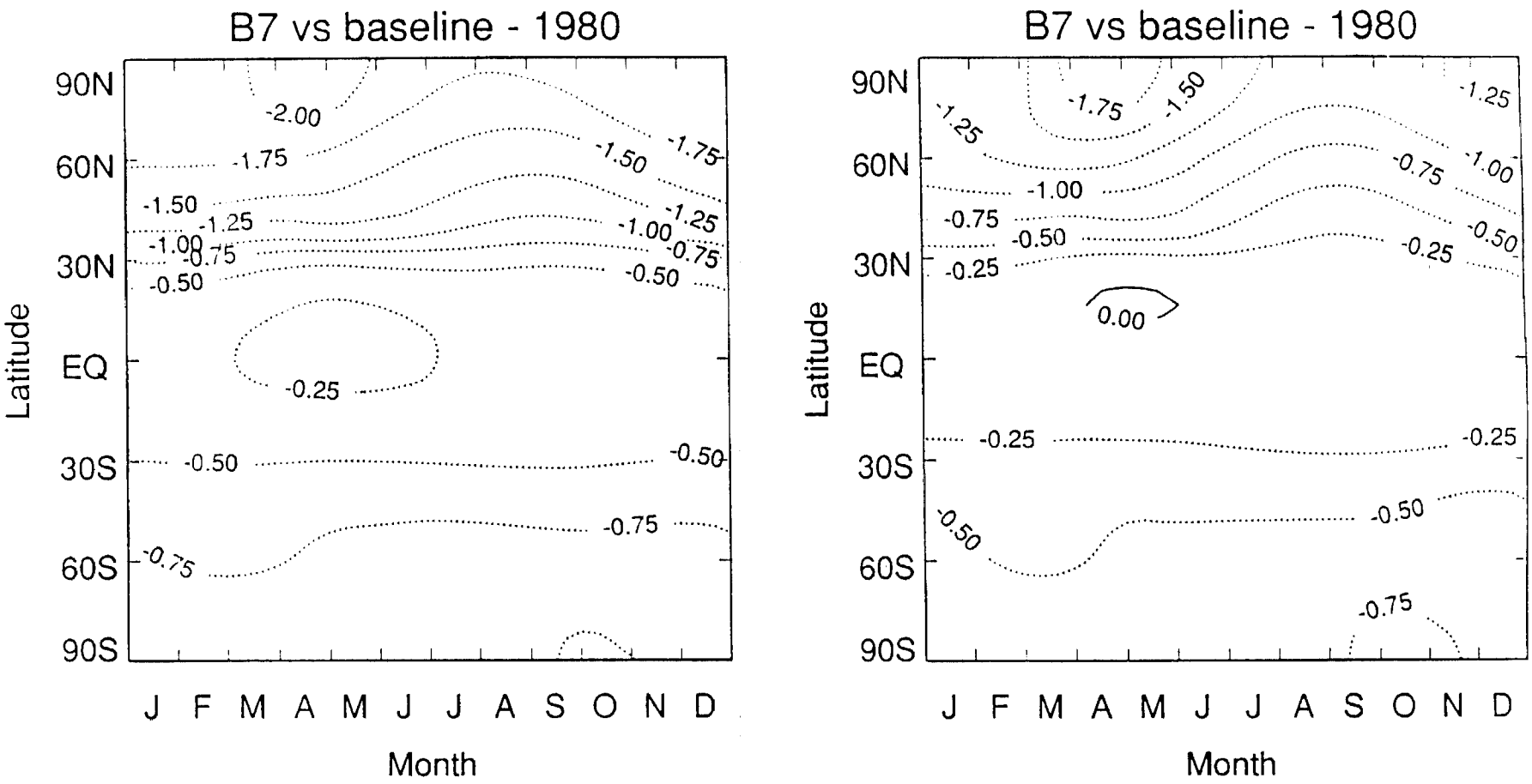

Figure 1. The calculated percent change in total ozone column from the 1980 baseline case for scenario B7, as a function of latitude and time of year with (a) the model used for previous results (Ko, et. al. 1989) and (b) the model used in this report.

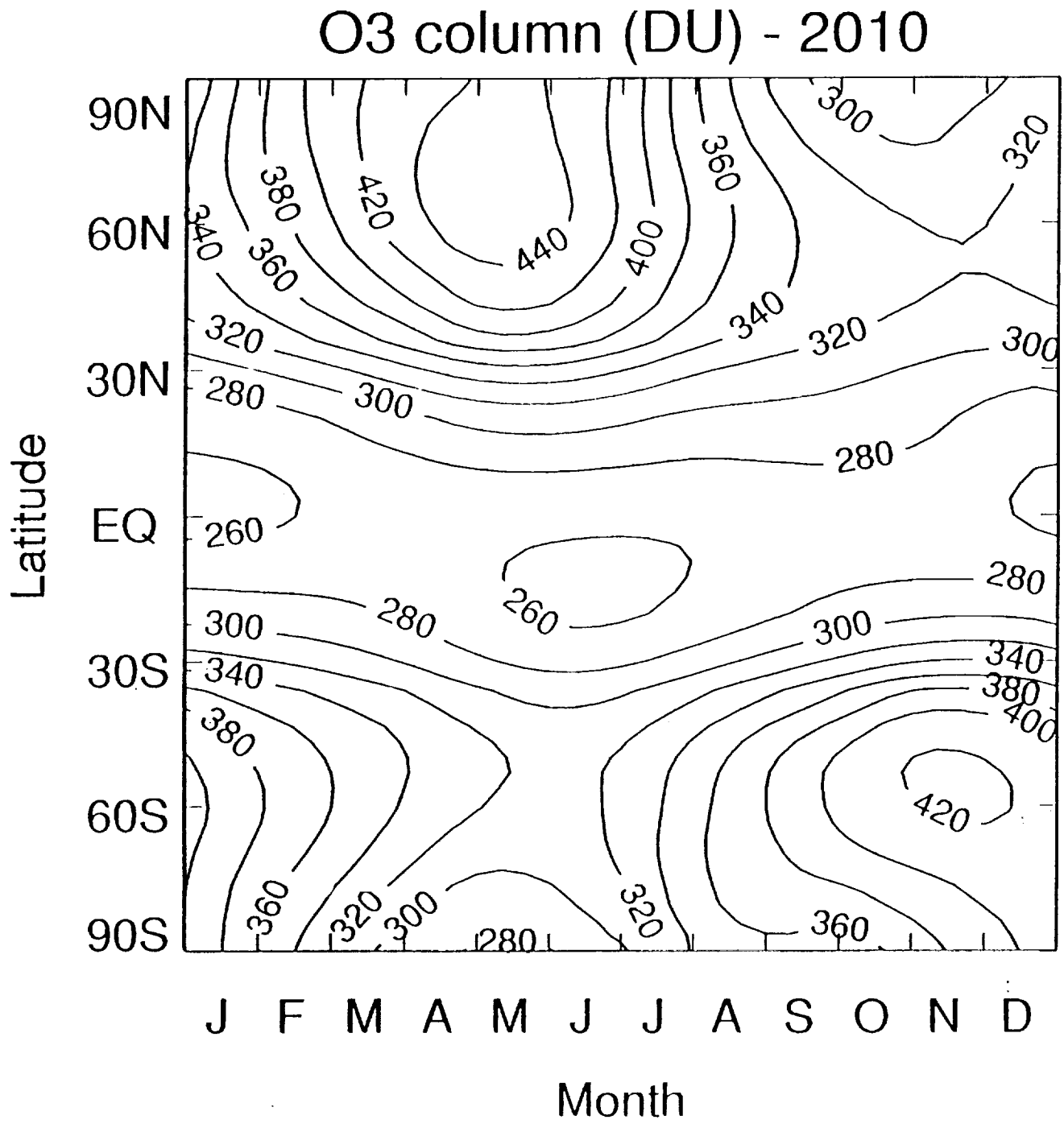

Figure 2. Total ozone column (Dobson units) as a function of latitude and time of year as calculated by the AER 2D chemical-transport model for the year 2010.

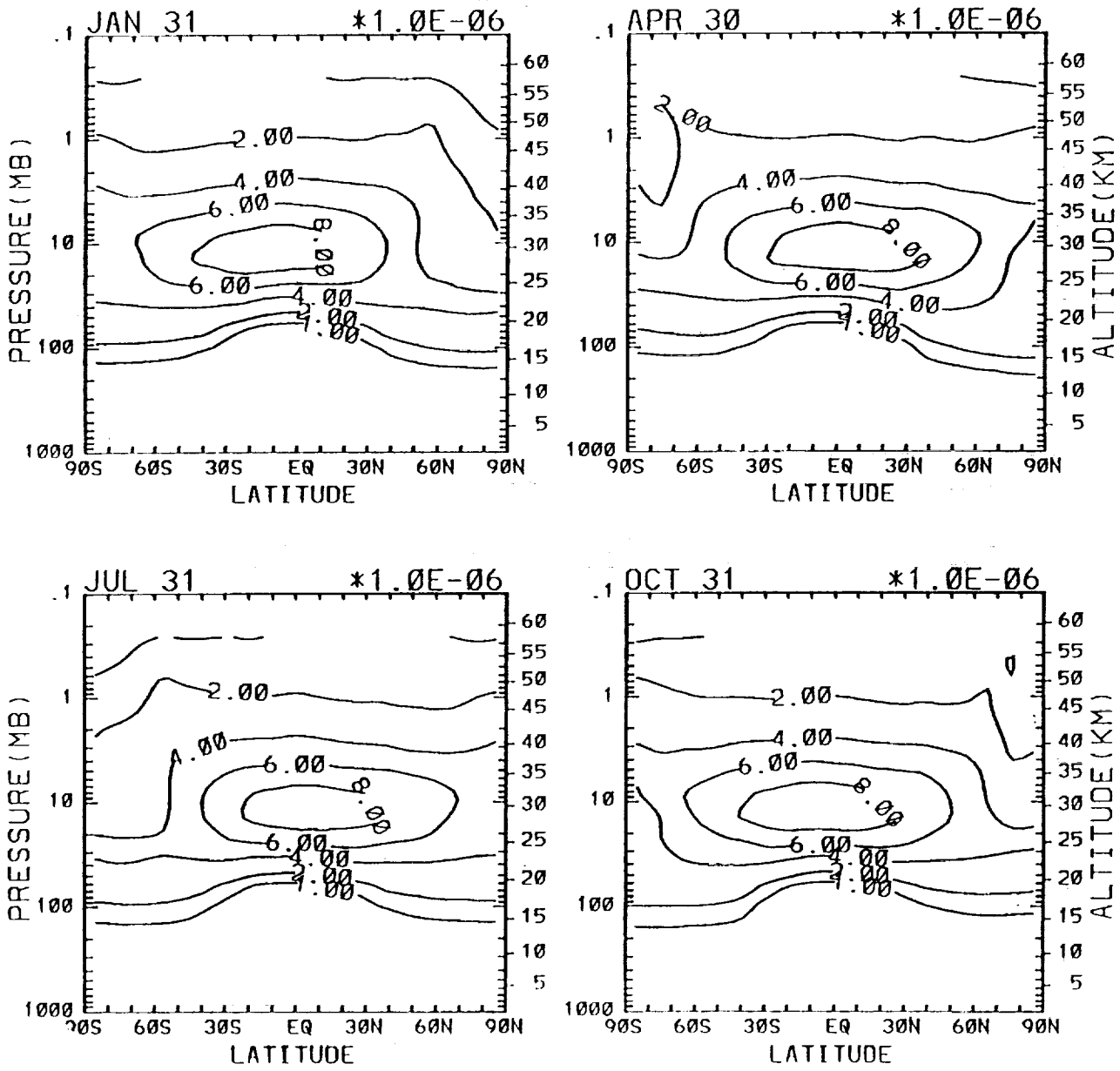

Figure 3. Model-calculated cross-sections of ozone mixing ratio (ppmv) as a function of latitude and height for (a) January, (b) April, (c) July, and (d) October for the year 2010. Contours are 1,2,4,6,8 ppmv.

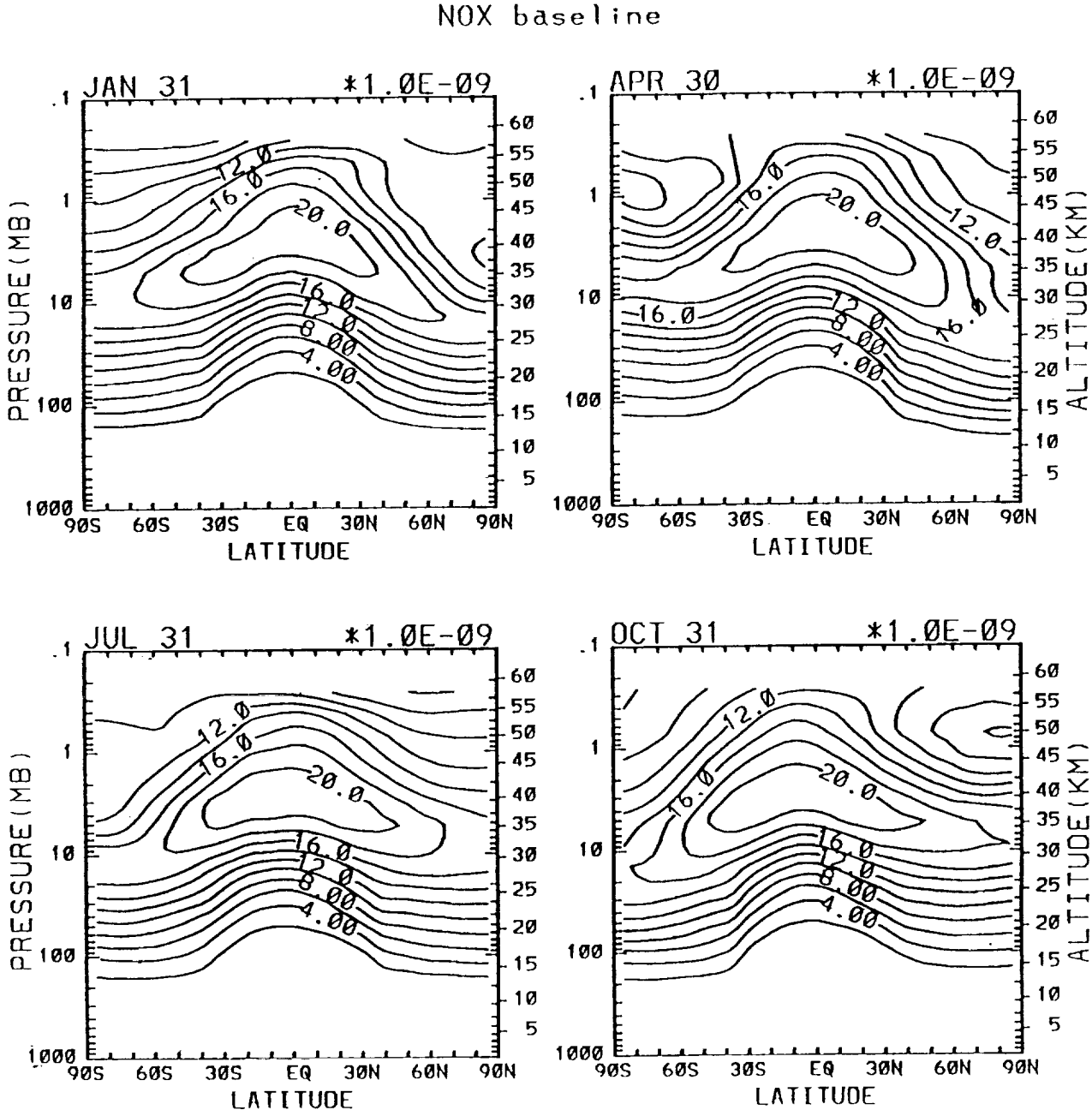

Figure 4. Model-calculated cross-sections of total odd nitrogen (NOY) mixing ratio (ppbv) as a function of latitude and height for (a) January, (b) April, (c) July, and (d) October for the year 2010. Contours are in 2 ppb increments.

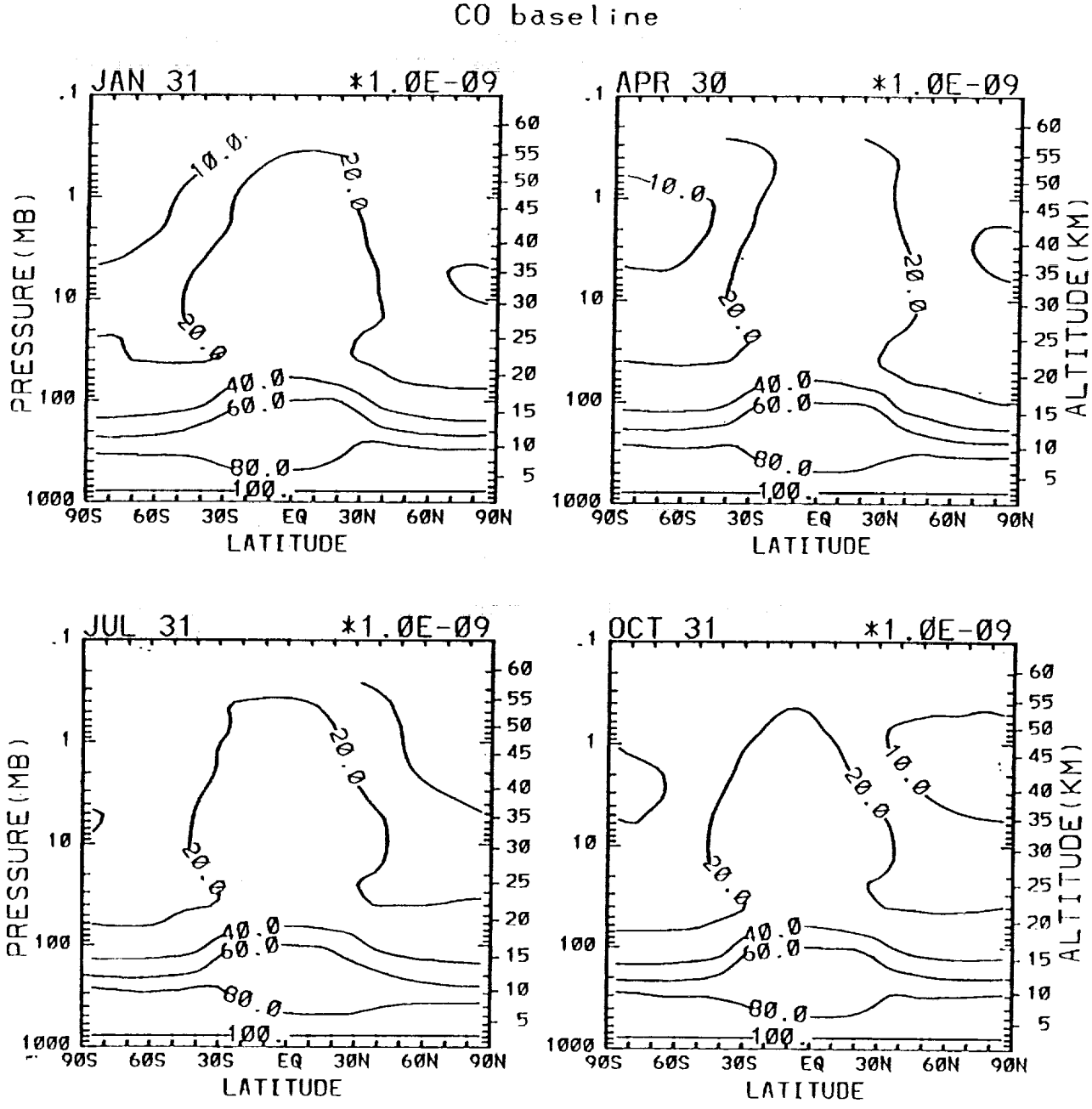

Figure 5. Model-calculated cross-sections of carbon monoxide (CO) mixing ratio (ppbv) as a function of latitude and height for (a) January, (b) April, (c) July, and (d) October for the year 2010. Contours are 10, 20, 40, 60, 80, 100 ppbv.

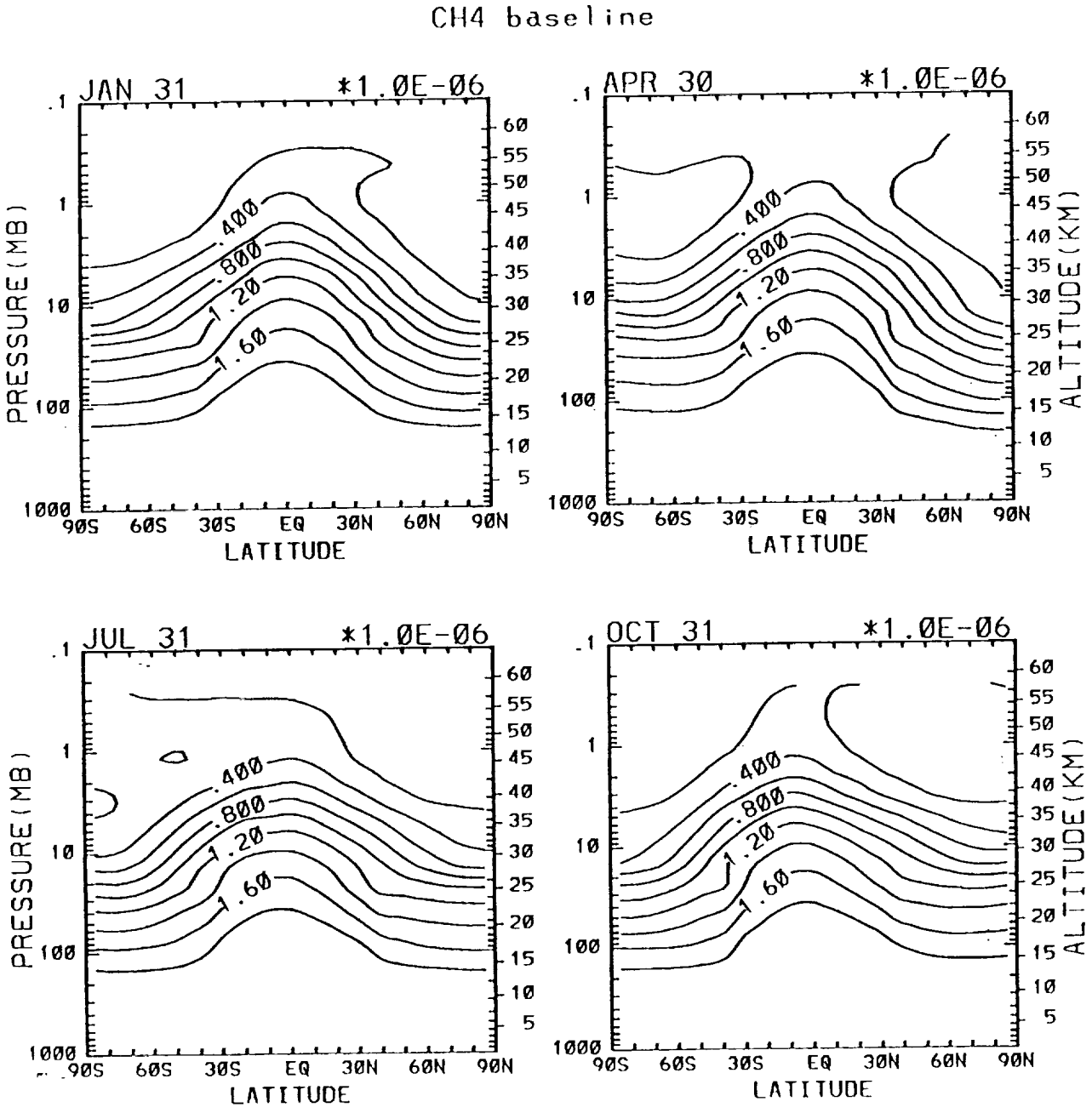

Figure 6. Model-calculated cross-sections of methane (CH_4) mixing ratio (ppbv) as a function of latitude and height for (a) January, (b) April, (c) July, and (d) October for the year 2010. Contours are in 0.2 ppmv increments.

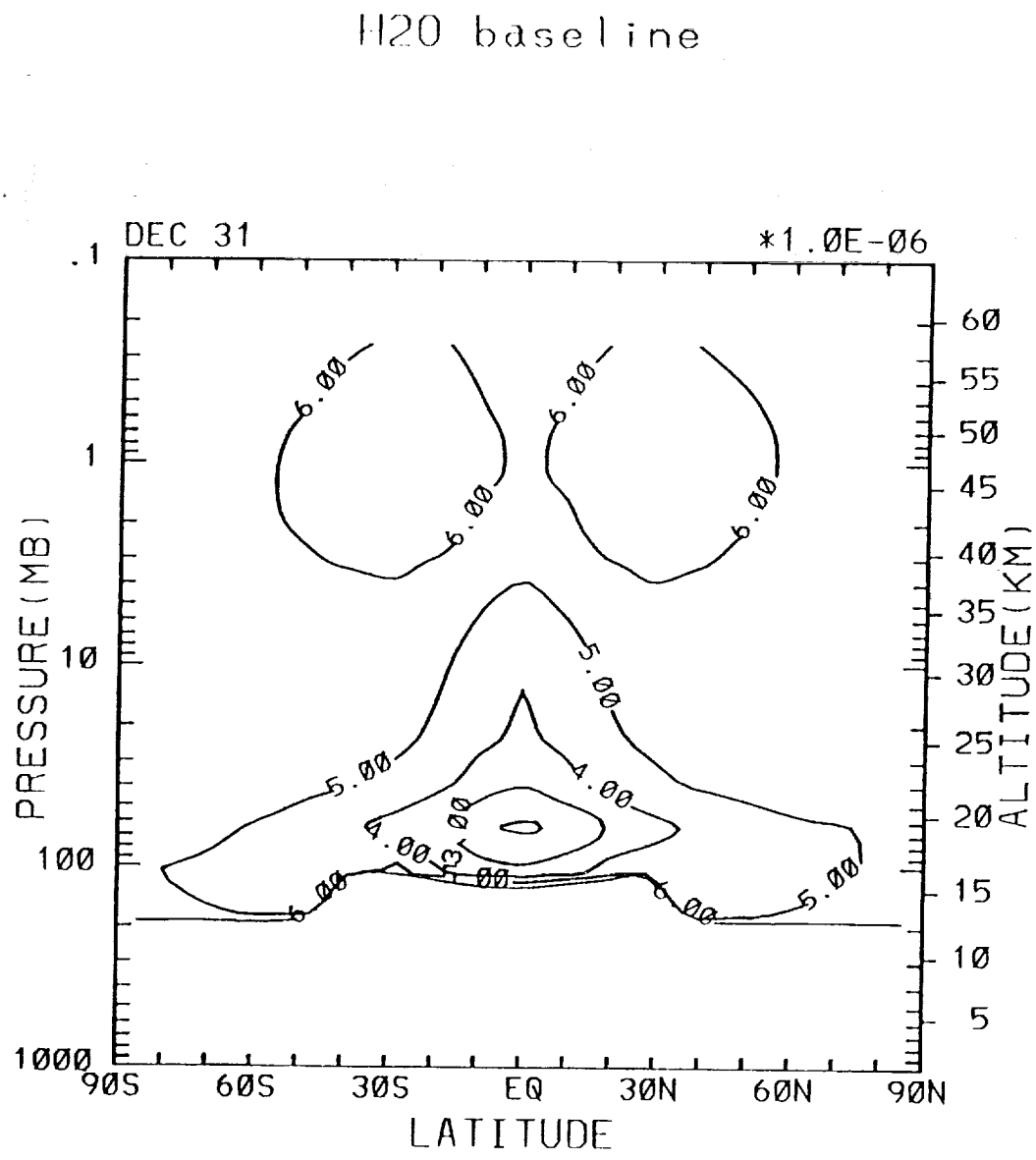

Figure 7. Stratospheric vapor (H_2O) concentration in ppmv as a function of latitude and height, derived from Remsberg, et al (1984), and adjusted to 2010 conditions by assuming that 2 additional H_2O molecules are produced by every CH_4 molecule in excess of 1985 concentrations dissociated above the tropopause.

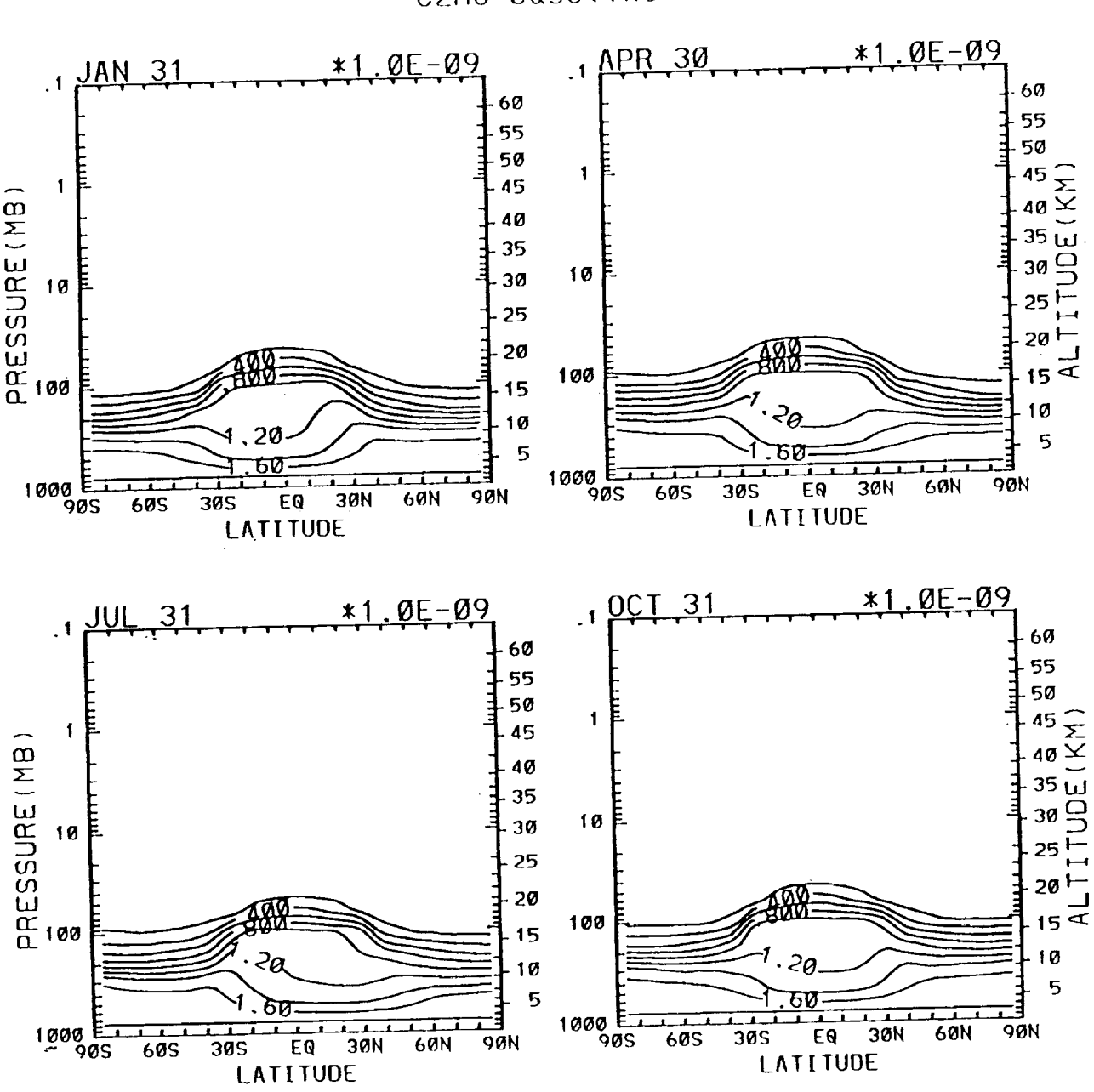

Figure 8. Model-calculated cross-sections of ethane (C_2H_6) mixing ratio (ppbv) as a function of latitude and height for (a) January, (b) April, (c) July, and (d) October for the year 2010. Contours are in increments of 0.2 ppbv.

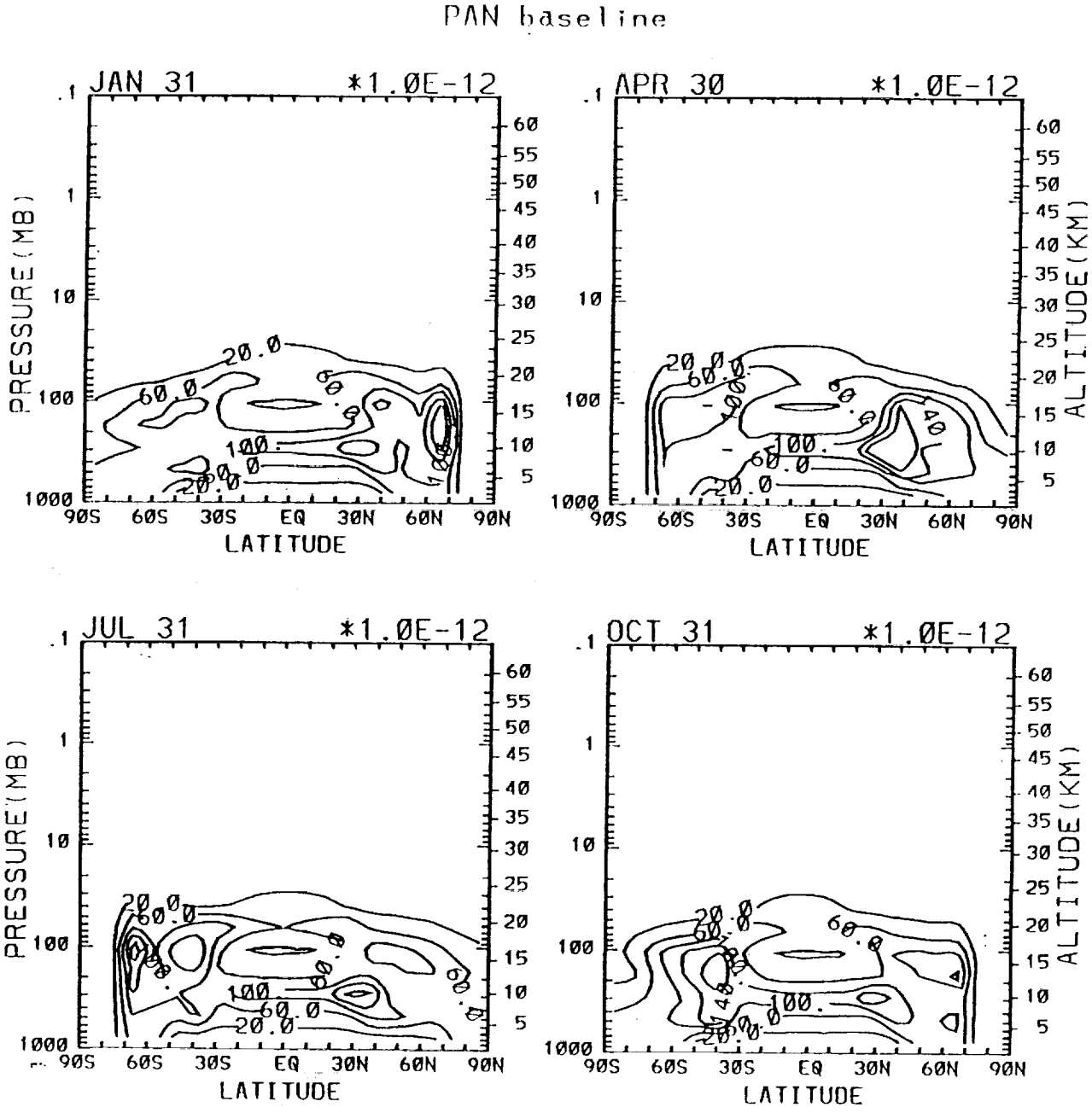

Figure 9. Model-calculated cross-sections of PAN ($CH_3CO_3NO_2$) mixing ratio (ppmv) as a function of latitude and height for (a) January, (b) April, (c) July, and (d) October for the year 2010. Contours are 20, 60, 100, 140, 180 pptv.

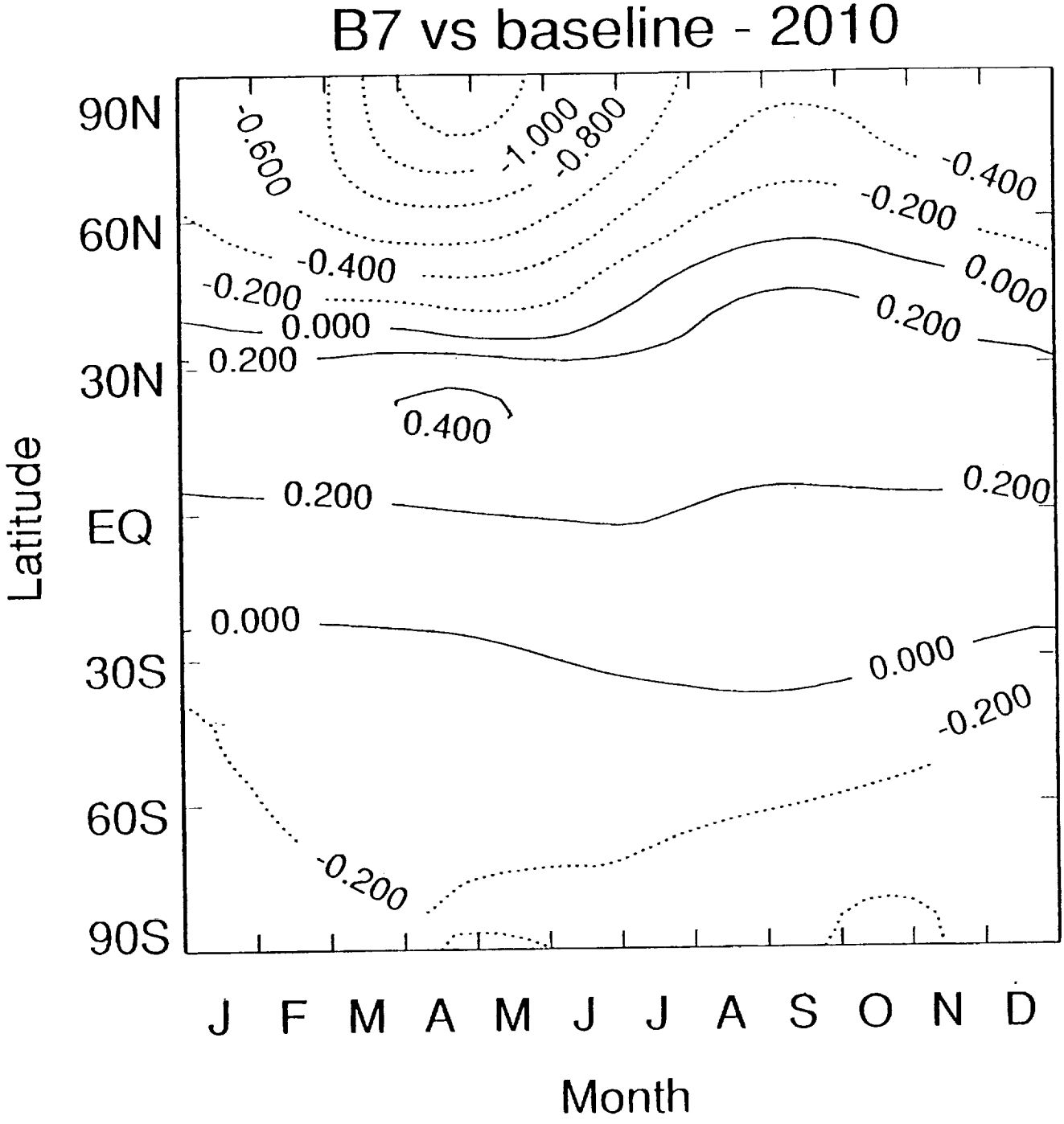

Figure 10. The calculated percent change in total ozone column from the 2010 baseline case for scenario B7, as a function of latitude and time of year.

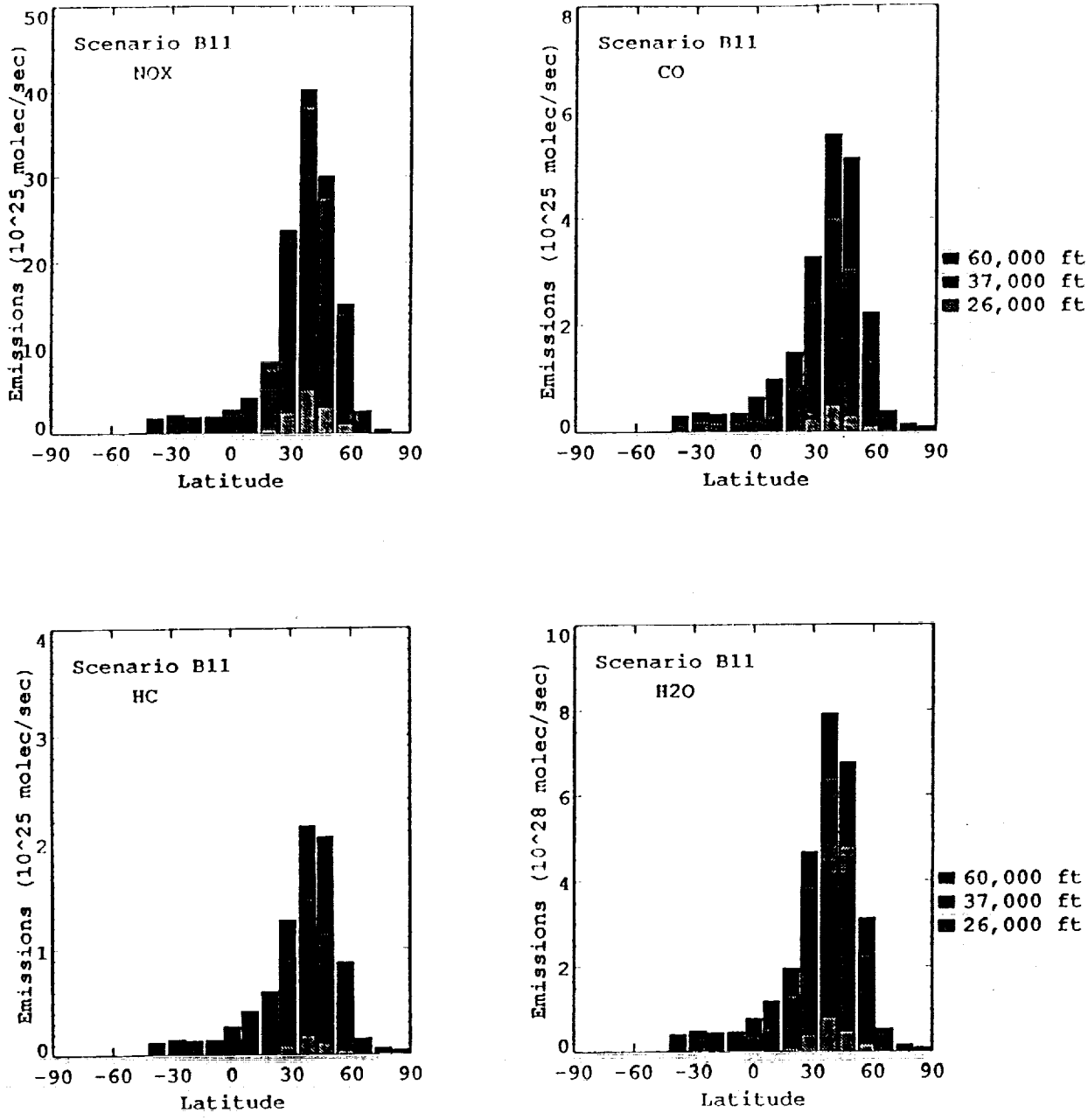

Figure 11. Emissions of (a) NOY, (b) CO, (c) hydrocarbon as CH_4, and (d) water vapor for Scenario B11 as a function of latitude. The height of the bar represents total emissions for the 9.5 degree latitude band in molecules per second. Shadings within bars represent the contribution to emissions from different model altitude levels.

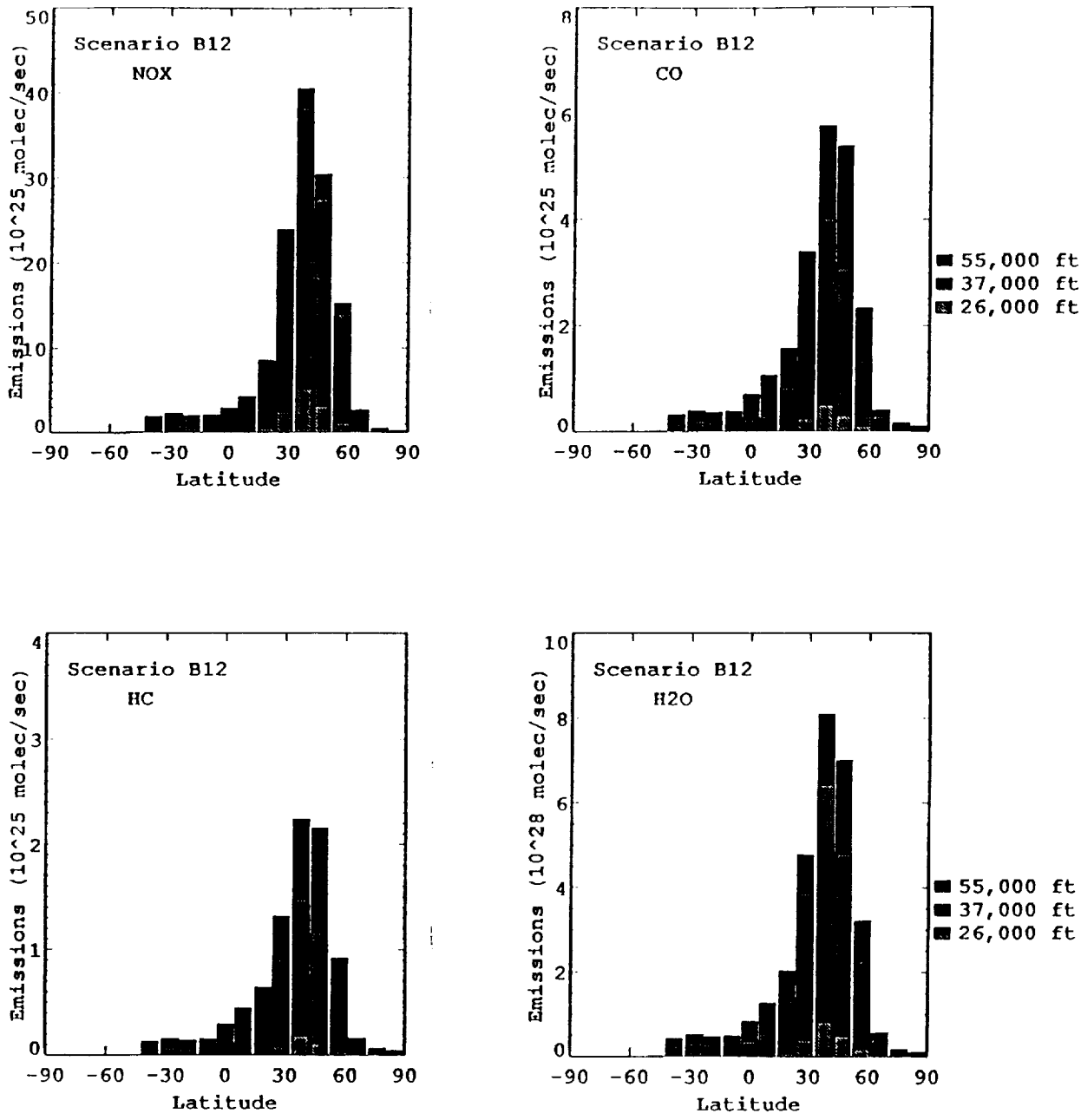

Figure 12. Emissions of (a) NOY, (b) CO, (c) hydrocarbon as CH_4, and (d) water vapor for Scenario B12 as a function of latitude. The height of the bar represents total emissions for the 9.5 degree latitude band in molecules per second. Shadings within bars represent the contribution to emissions from different model altitude levels.

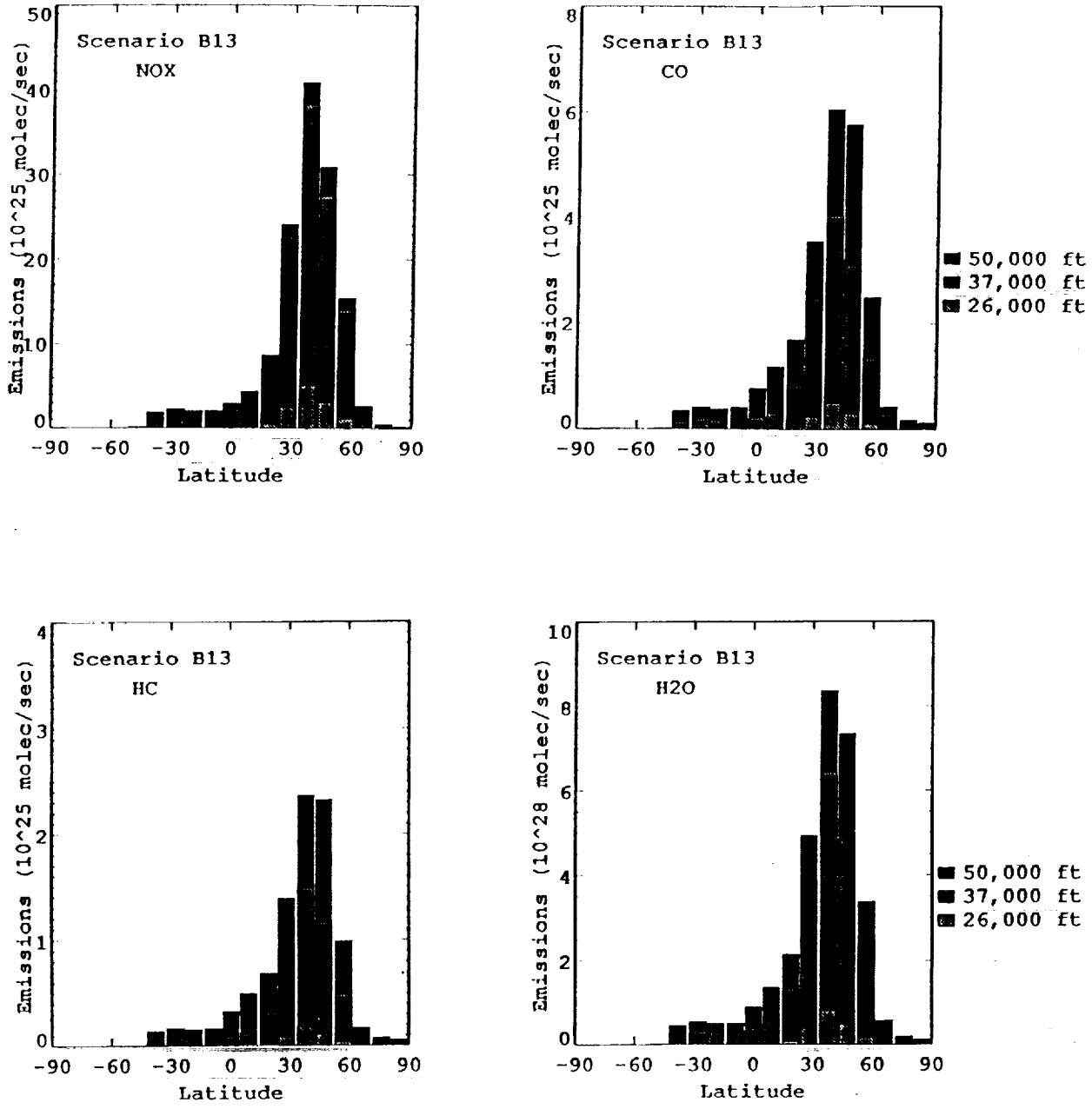

Figure 13. Emissions of (a) NOY, (b) CO, (c) hydrocarbon as CH_4, and (d) water vapor for Scenario B13 as a function of latitude. The height of the bar represents total emissions for the 9.5 degree latitude band in molecules per second. Shadings within bars represent the contribution to emissions from different model altitude levels.

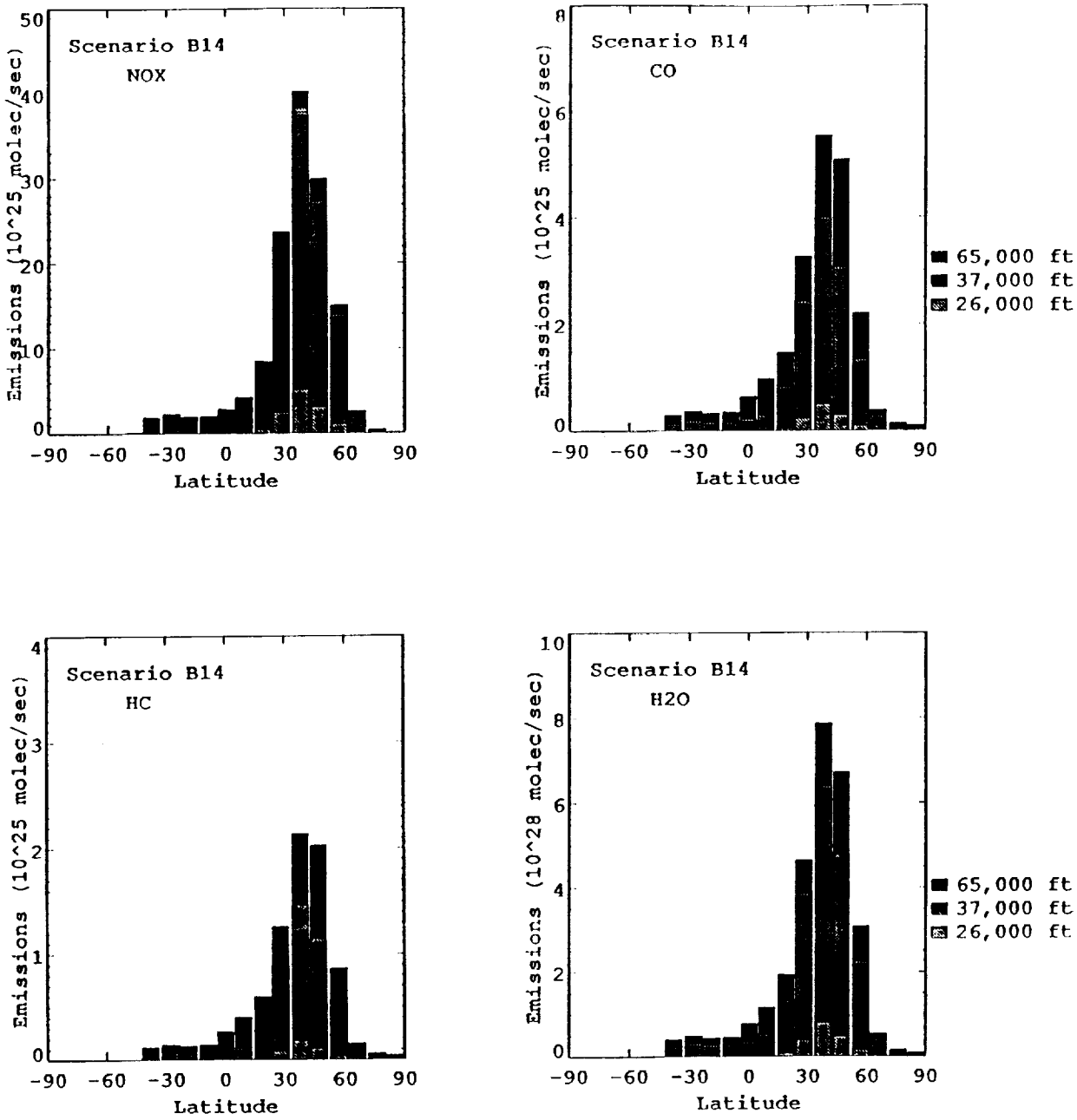

Figure 14. Emissions of (a) NOY, (b) CO, (c) hydrocarbon as CH_4, and (d) water vapor for Scenario B14 as a function of latitude. The height of the bar represents total emissions for the 9.5 degree latitude band in molecules per second. Shadings within bars represent the contribution to emissions from different model altitude levels.

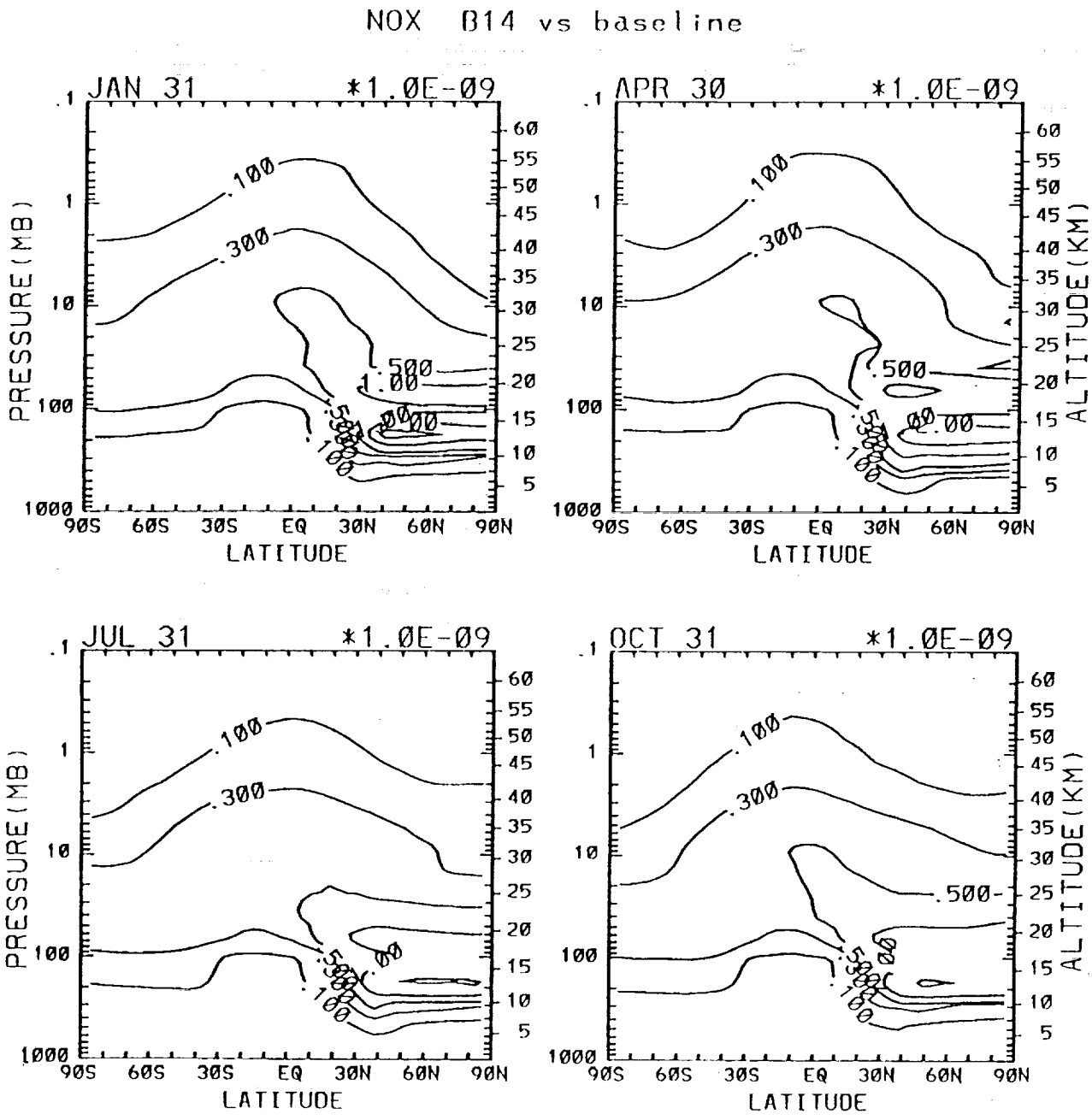

Figure 15. The calculated change in NOY in ppbv from the baseline case for scenario B14, as a function of latitude and altitude, for (a) January, (b) April, (c) July, and (d) October. Contour levels are 0.1, 0.3, 0.5, 1, 2, 3 ppbv.

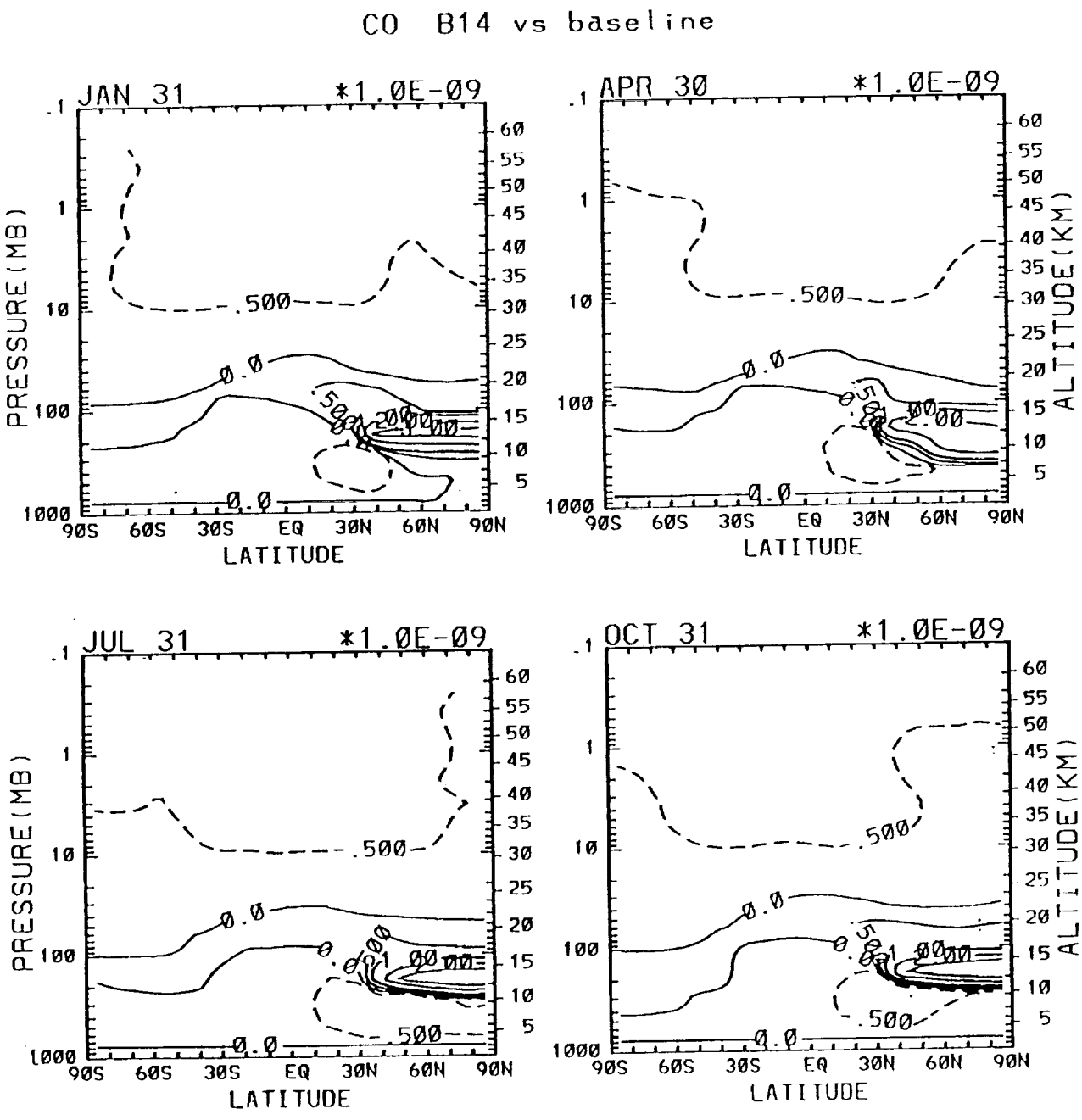

Figure 16. The calculated change in CO in ppbv from the baseline case for scenario B14, as a function of latitude and altitude, for (a) January, (b) April, (c) July, and (d) October. Contour levels are -.5, 0.5, 1, 2, 3 ppbv.

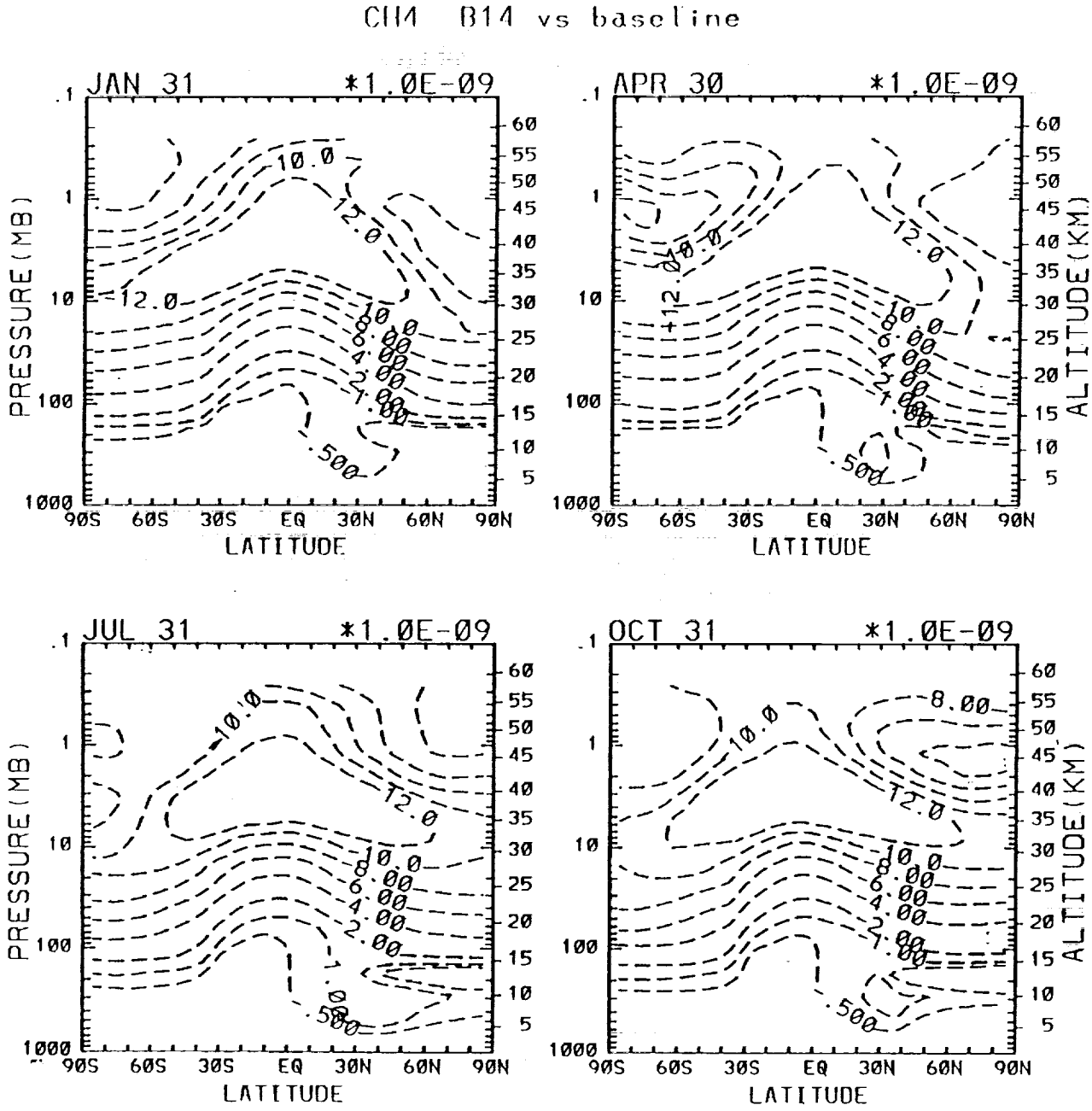

Figure 17. The calculated change in CH_4 in ppbv from the baseline case for scenario B14, as a function of latitude and altitude, for (a) January, (b) April, (c) July, and (d) October. Contour levels are -.5, -1, -2, -4, -6, -8, -10, -12, ppbv.

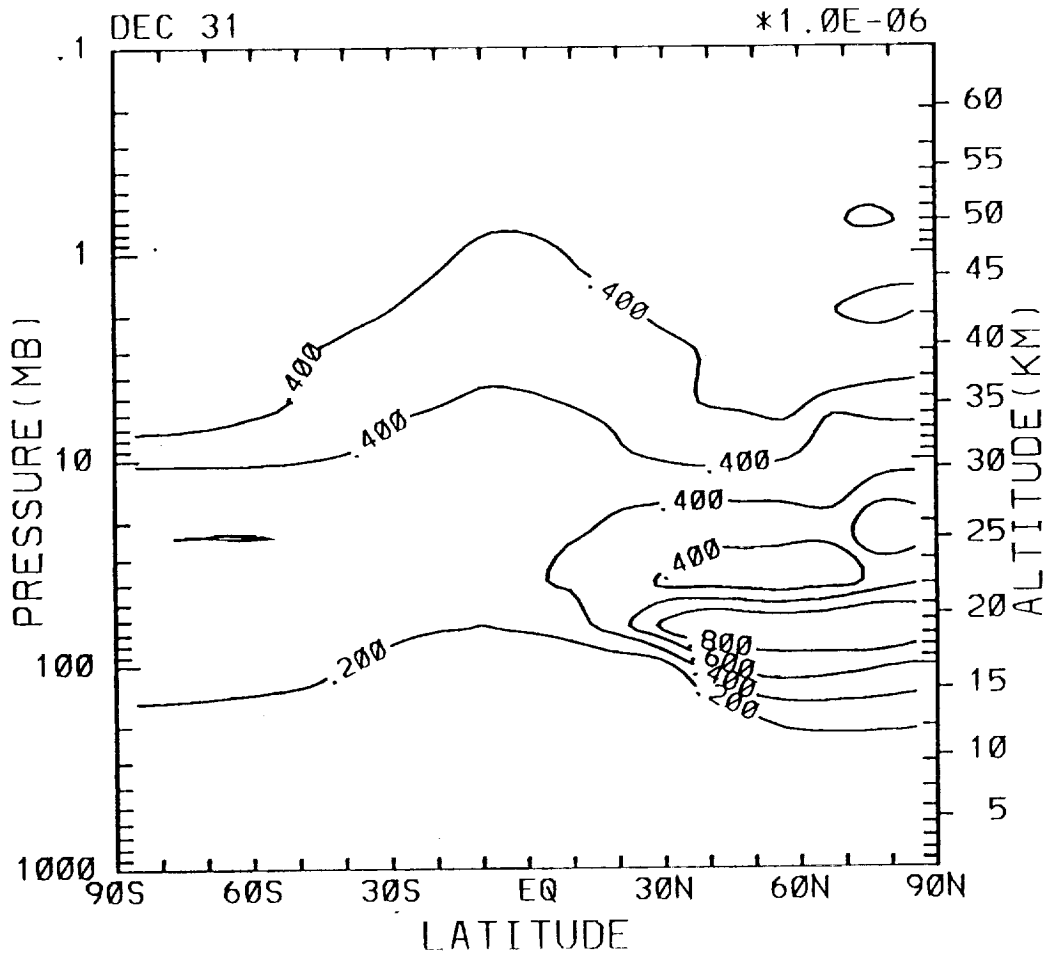

Figure 18. The calculated change in H_2O in ppbv from the baseline case for scenario B14, as a function of latitude and altitude, for (a) January, (b) April, (c) July, and (d) October. Contour levels are 0.2, 0.4, 0.6, 0.8 ppmv.

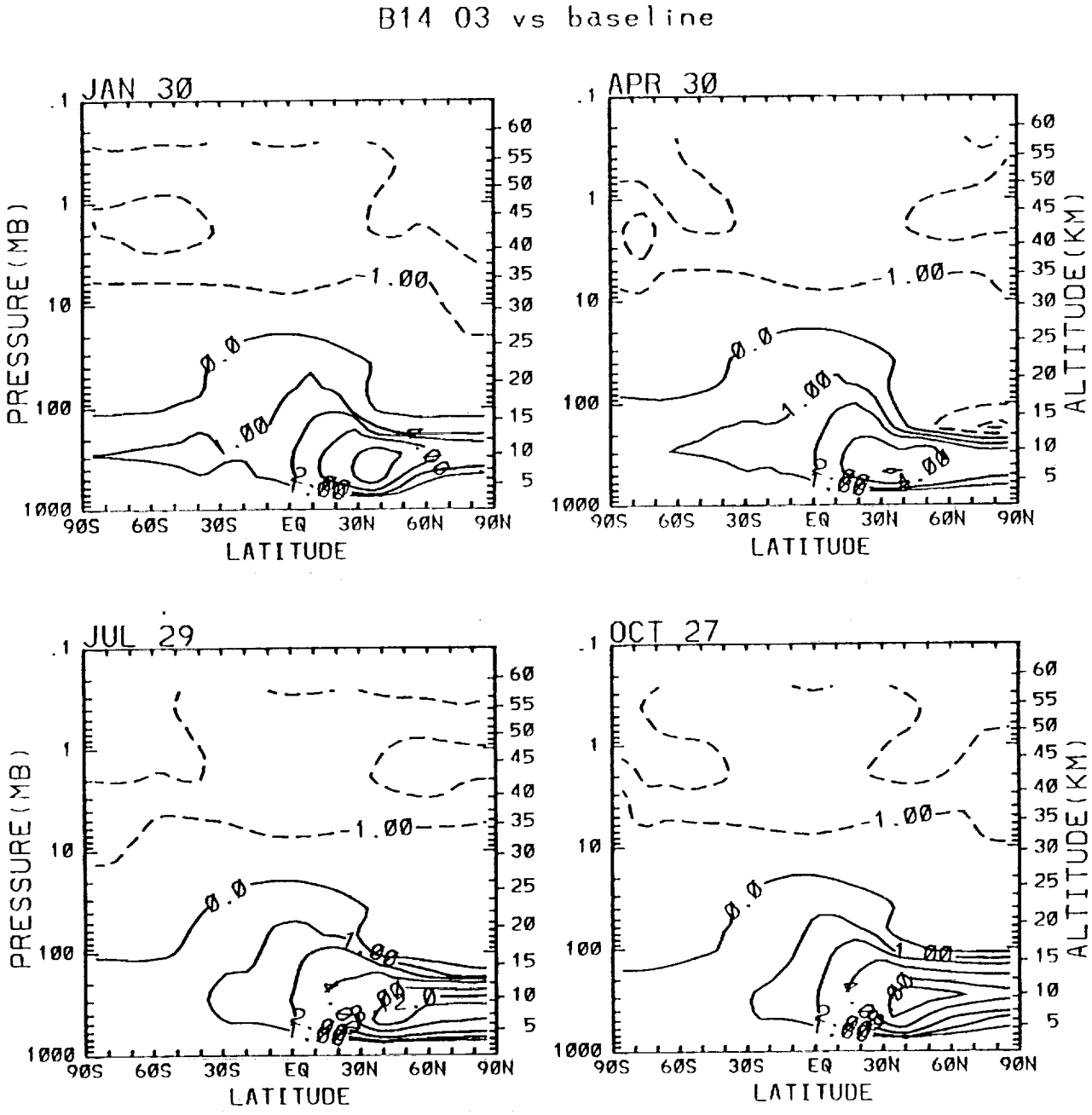

Figure 19. The calculated percent change in O_3 mixing ratio in ppbv from the baseline case for scenario B14, as a function of latitude and altitude, for (a) January, (b) April, (c) July, and (d) October. Contour levels are -2, -1, 0, 1, 2, 4, 8, 12% ppbv.

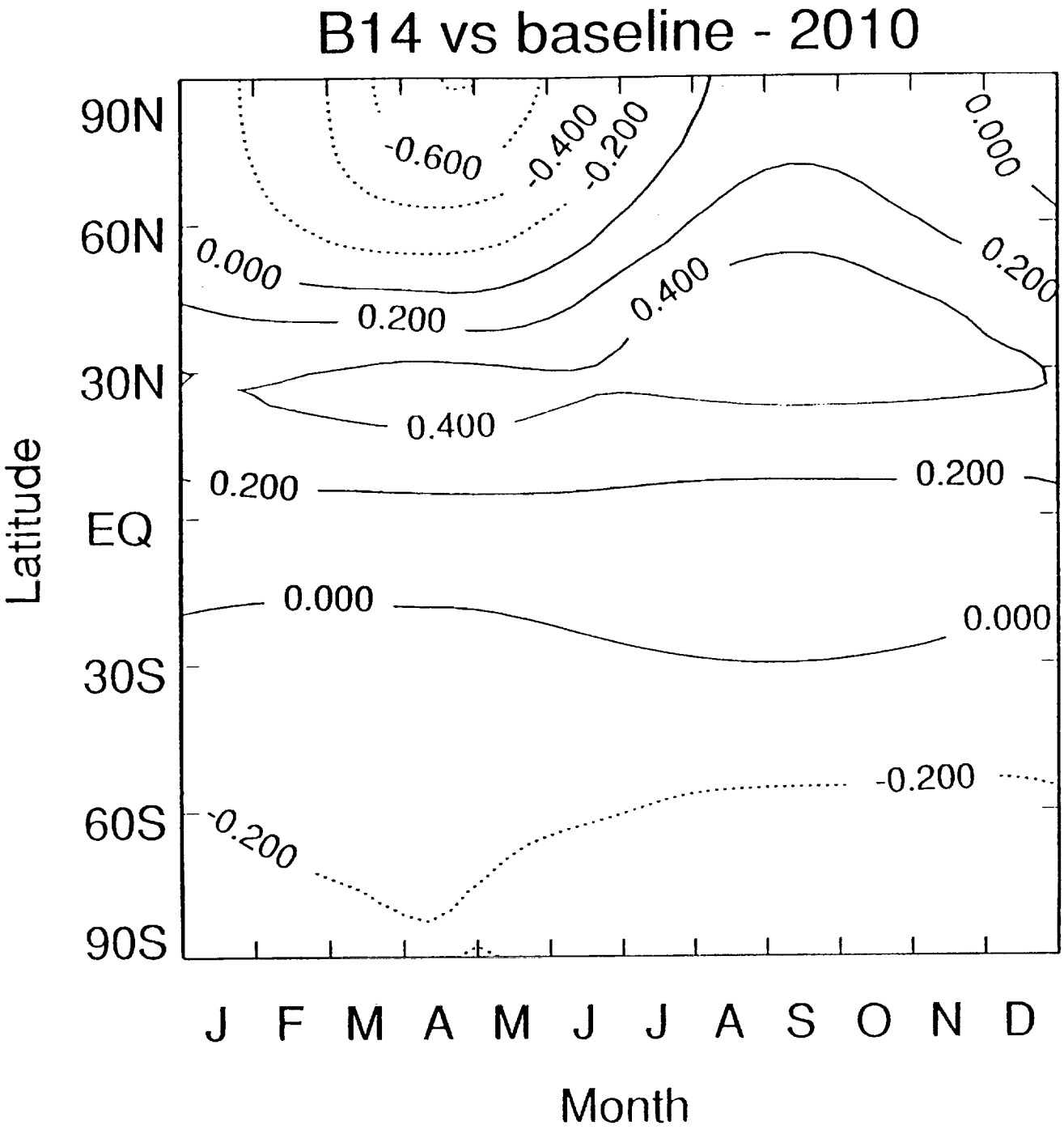

Figure 20. The calculated percent change in total ozone column from the baseline case for scenario B14, as a function of latitude and time of year. Contours are from -0.8 to 0.4 % in 0.2% increments.

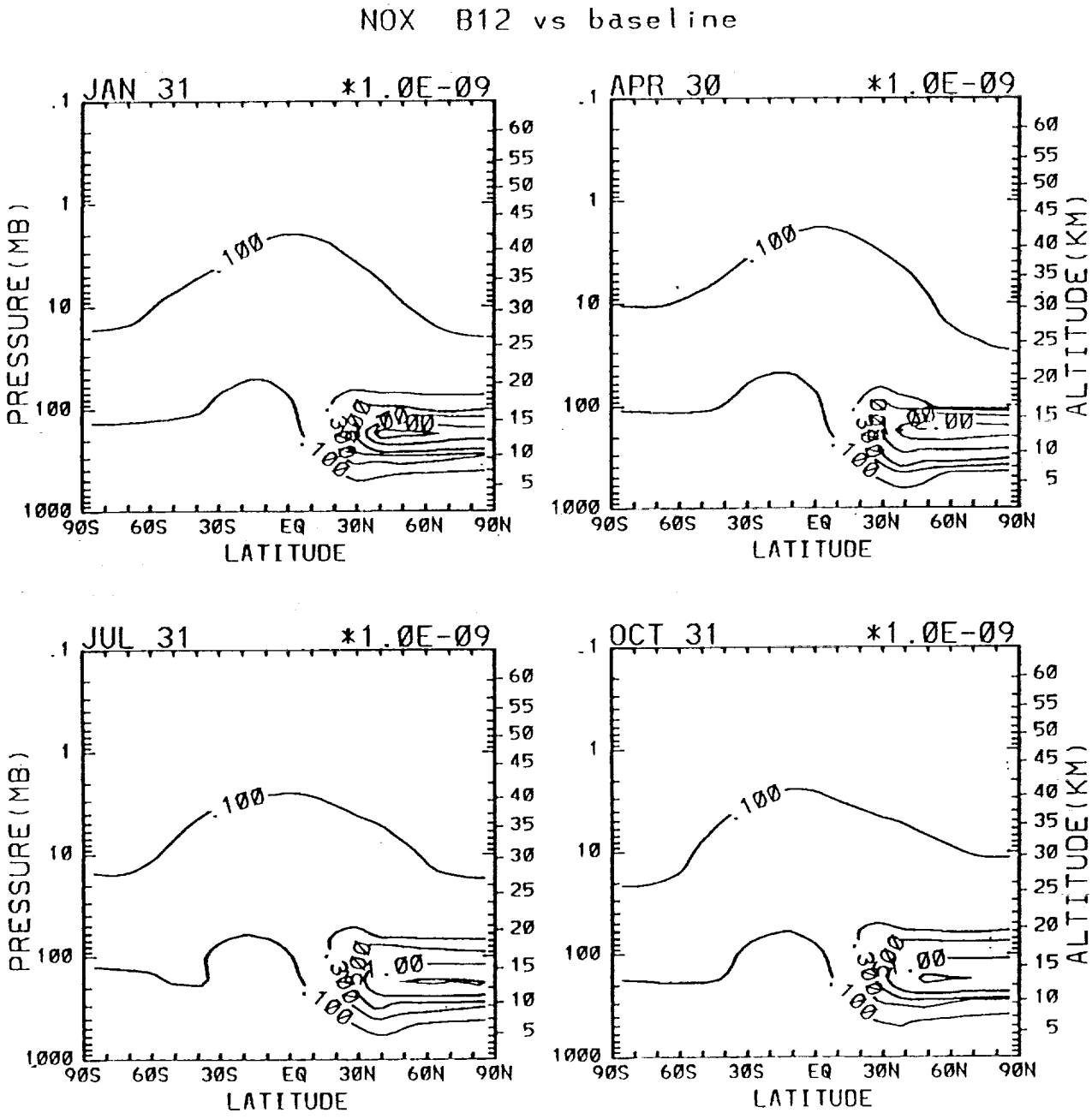

Figure 21. The calculated change in NOY in ppbv from the baseline case for scenario B12, as a function of latitude and altitude, for (a) January, (b) April, (c) July, and (d) October. Contour levels are 0.1, 0.3, 0.5, 1, 2, 3 ppbv.

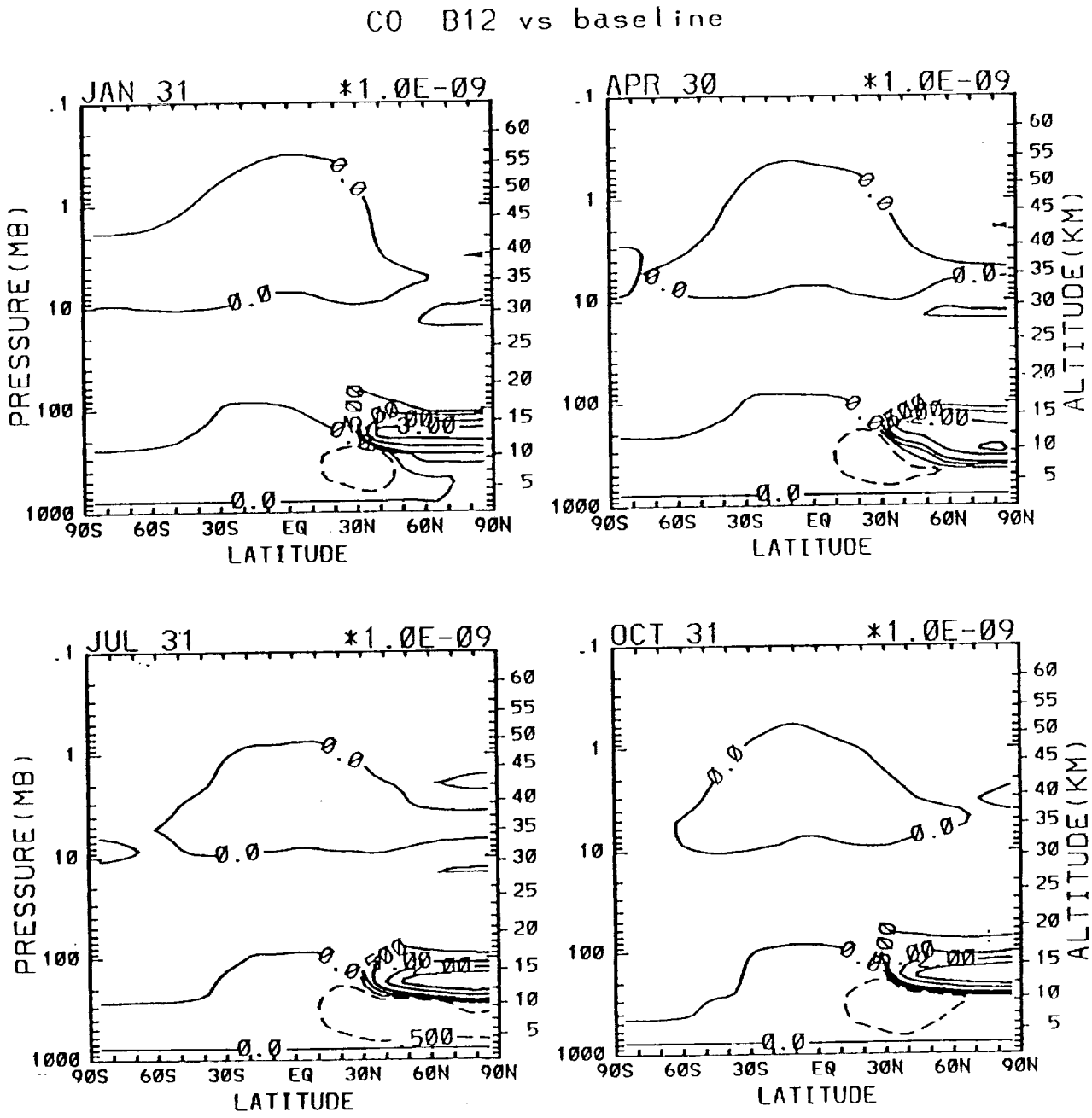

Figure 22. The calculated change in CO in ppbv from the baseline case for scenario B12, as a function of latitude and altitude, for (a) January, (b) April, (c) July, and (d) October. Contour levels are -0.5, 0, 0.5, 1, 2, 3 ppbv.

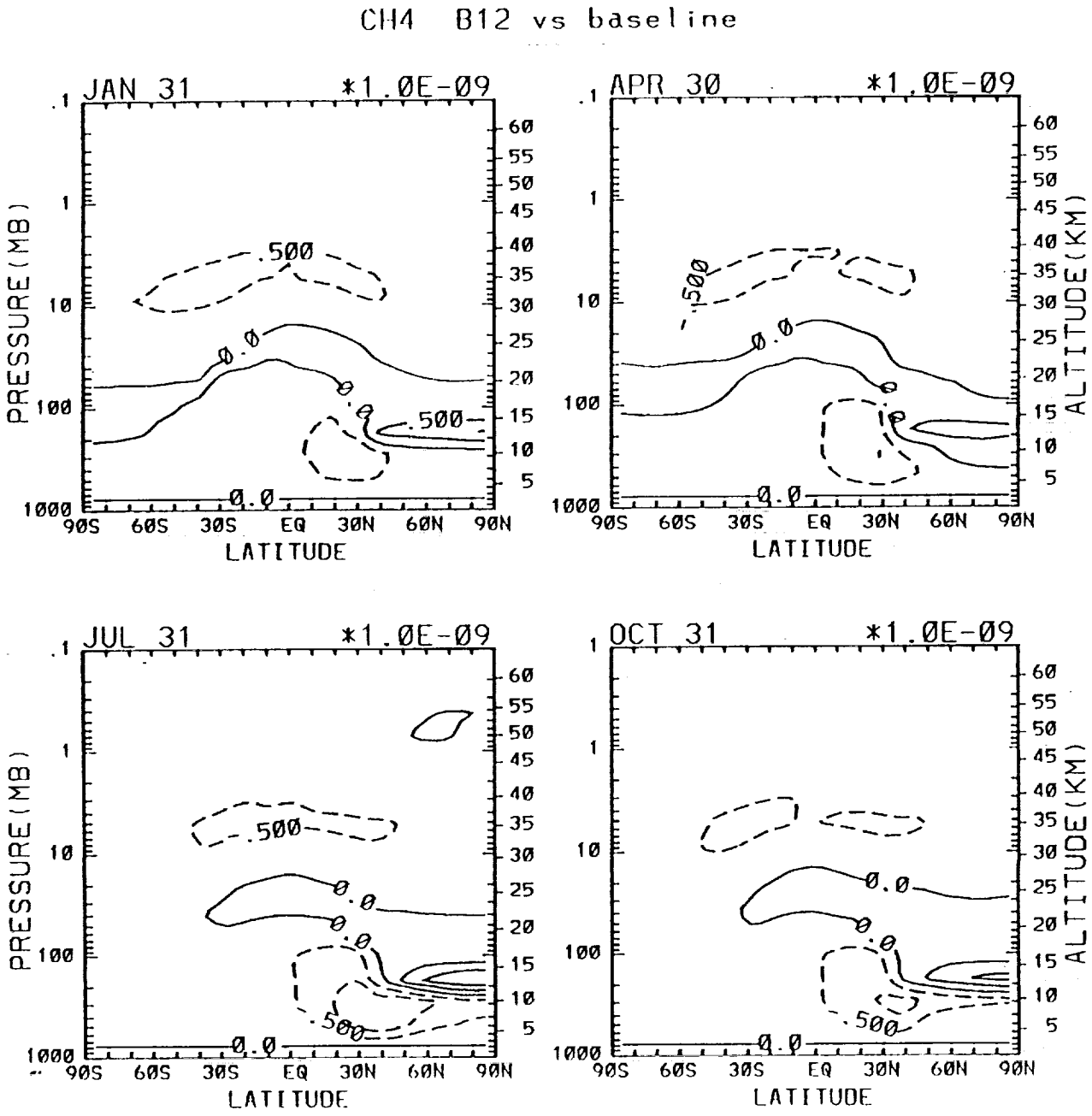

Figure 23. The calculated change in CH_4 in ppbv from the baseline case for scenario B12, as a function of latitude and altitude, for (a) January, (b) April, (c) July, and (d) October. Contour levels are -1, -.5, 0, 0.5, 1, 2 ppbv.

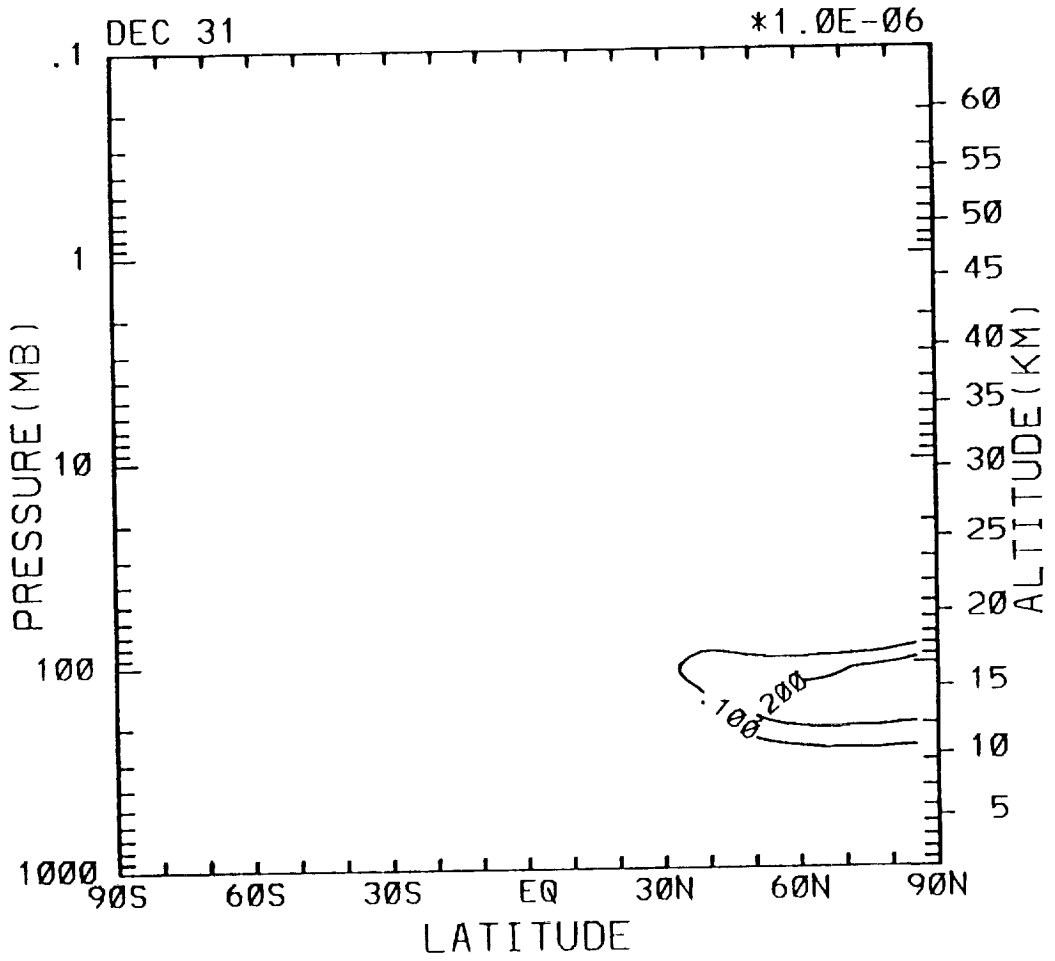

Figure 24. The calculated change in H_2O in ppbv from the baseline case for scenario B12, as a function of latitude and altitude, for (a) January, (b) April, (c) July, and (d) October. Contour levels are 0.1, 0.2 ppmv.

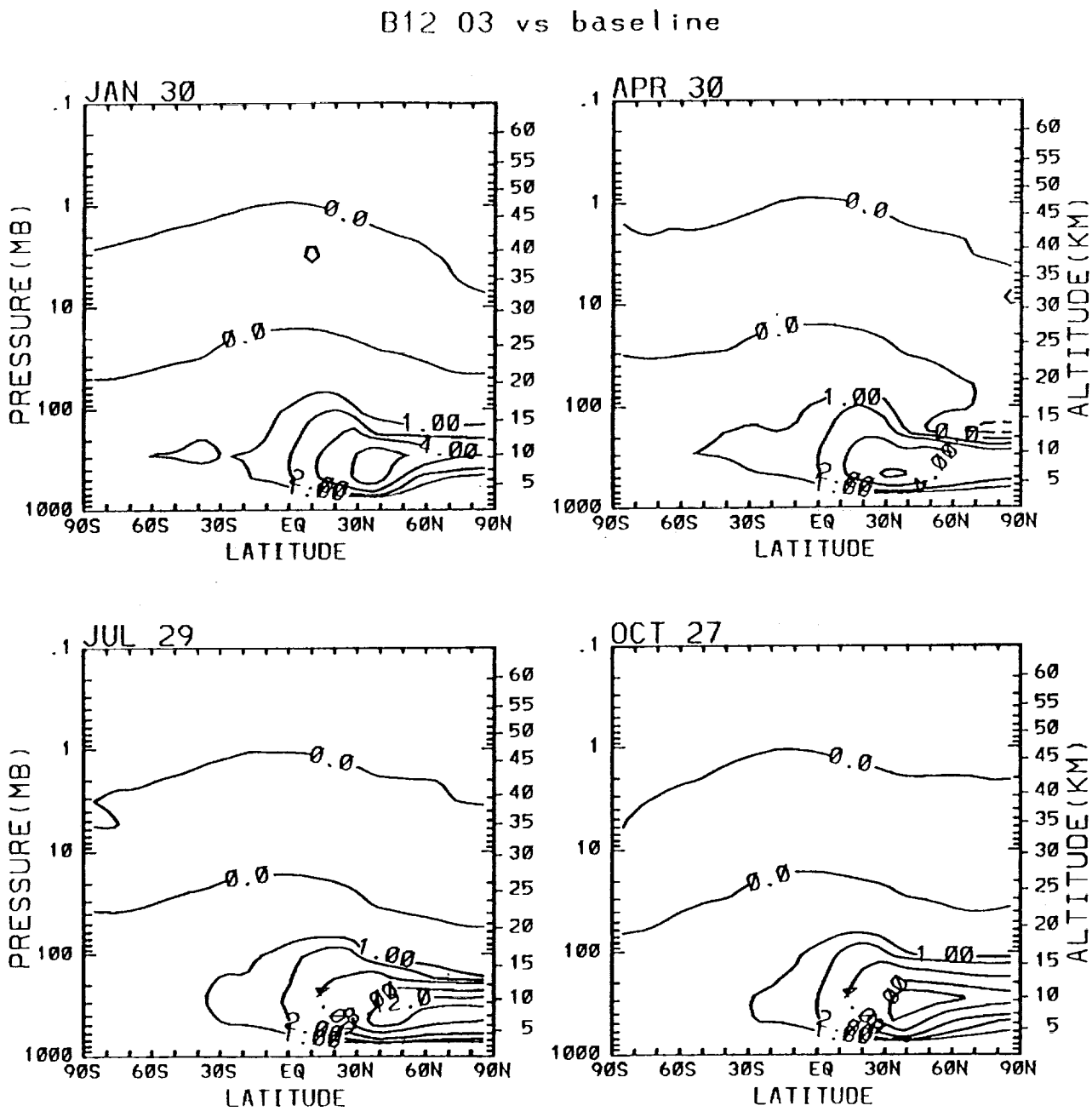

Figure 25. The calculated percent change in O_3 mixing ratio in ppbv from the baseline case for scenario B12, as a function of latitude and altitude, for (a) January, (b) April, (c) July, and (d) October. Contour levels are 0, 1, 2, 4, 8, 12% ppbv.

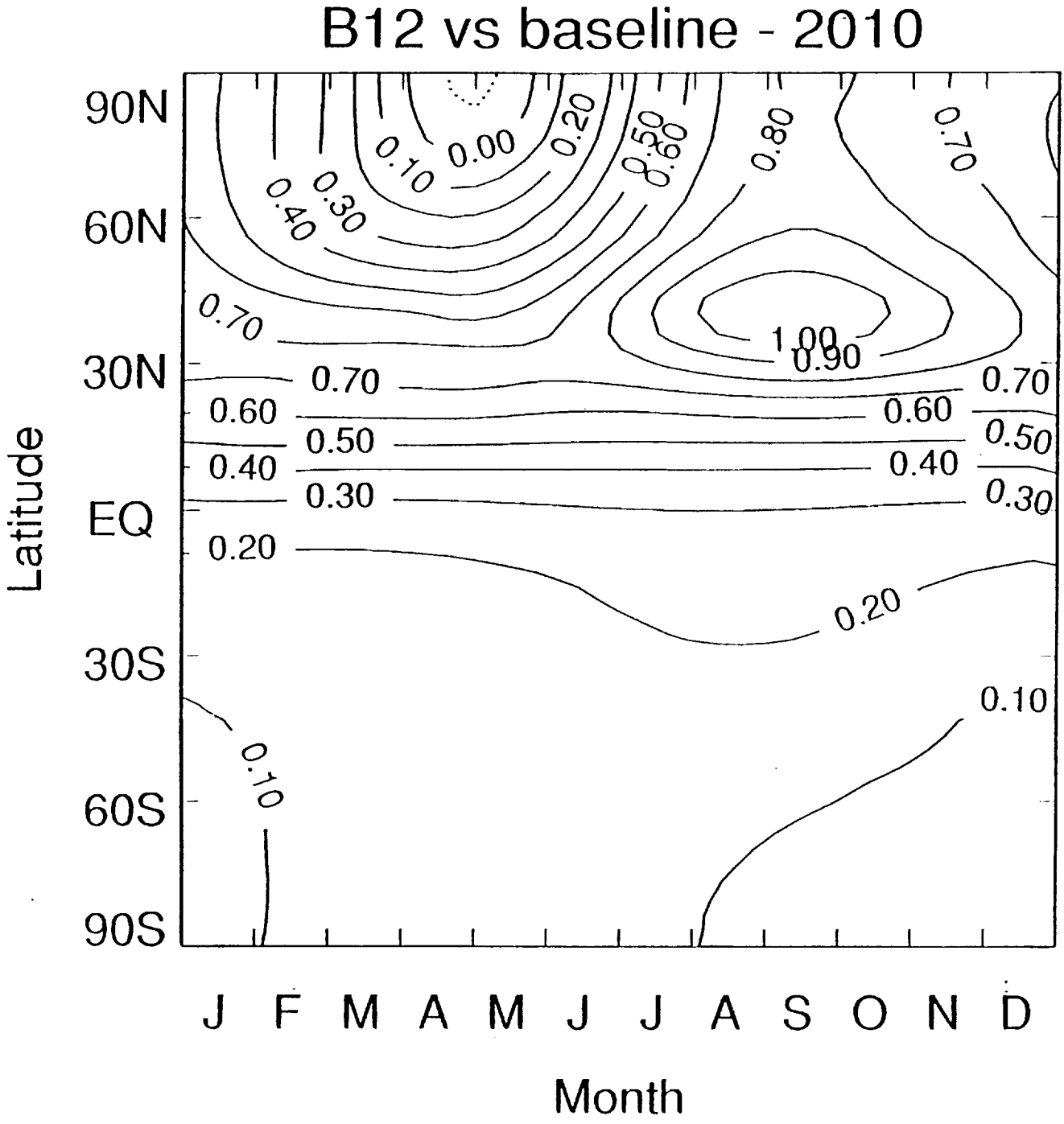

Figure 26. The calculated percent change in total ozone column from the baseline case for scenario B12, as a function of latitude and time of year. Contours are from -0.1% to +0.1 % in increments of 0.1%.

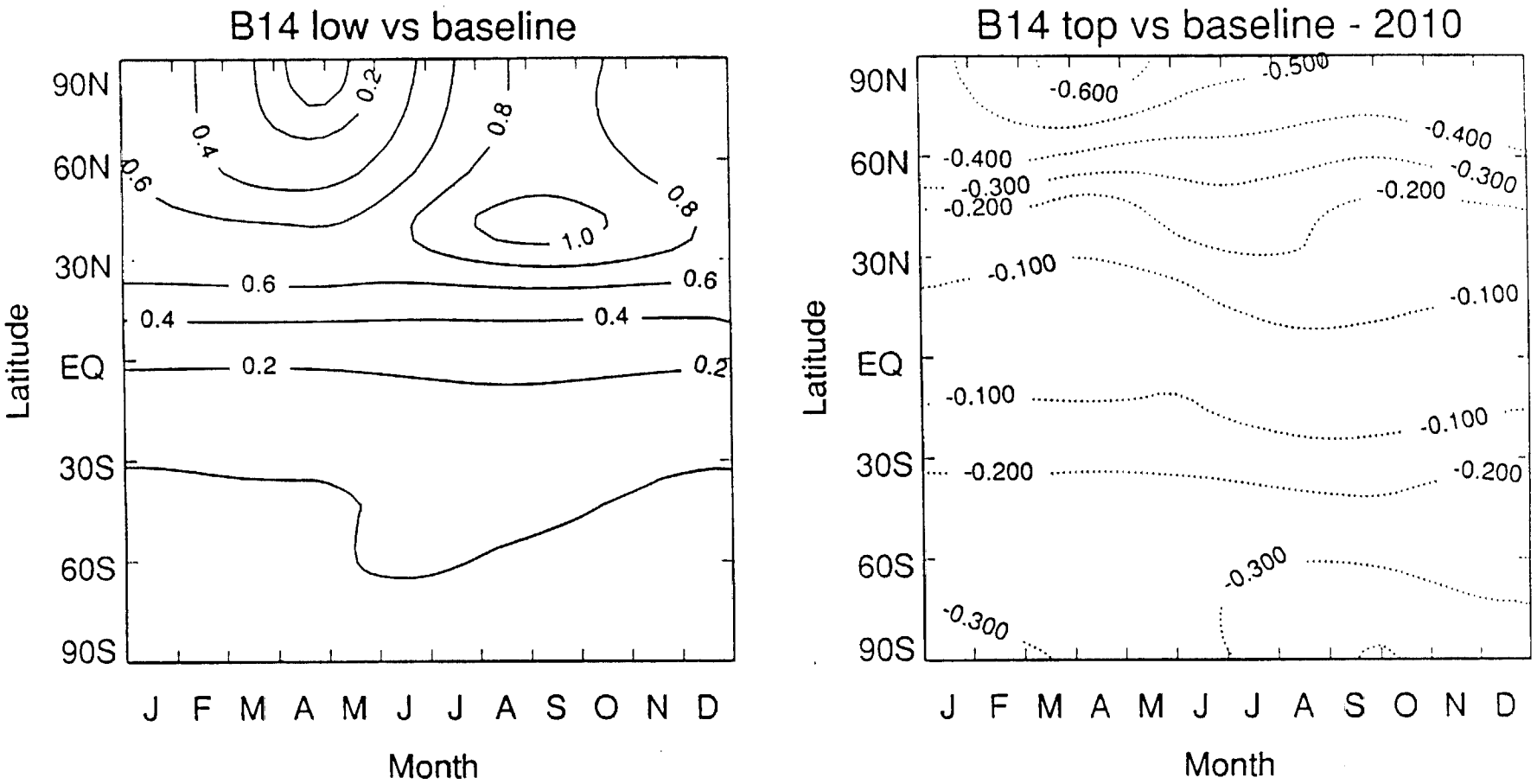

Figure 27. The calculated percent change in total ozone column from the baseline case for (a) scenario B14 emissions below 40000 ft and (b) B14 emissions at 65000 ft only, as a function of latitude and time of year.

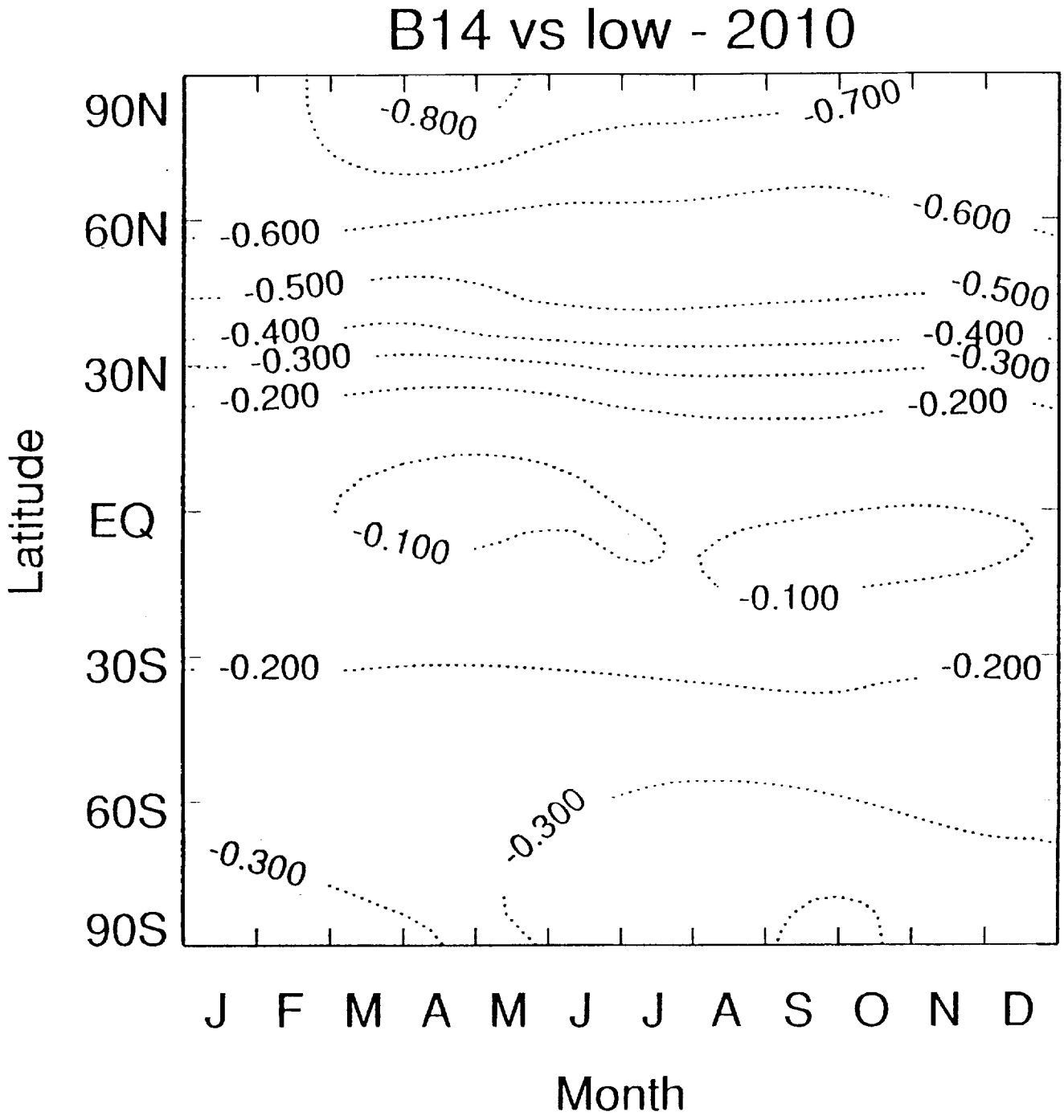

Figure 28. The calculated change in total ozone column for scenario B14 with emissions at all levels as a percentage of the ozone column with scenario B14 emissions below 40000 ft.

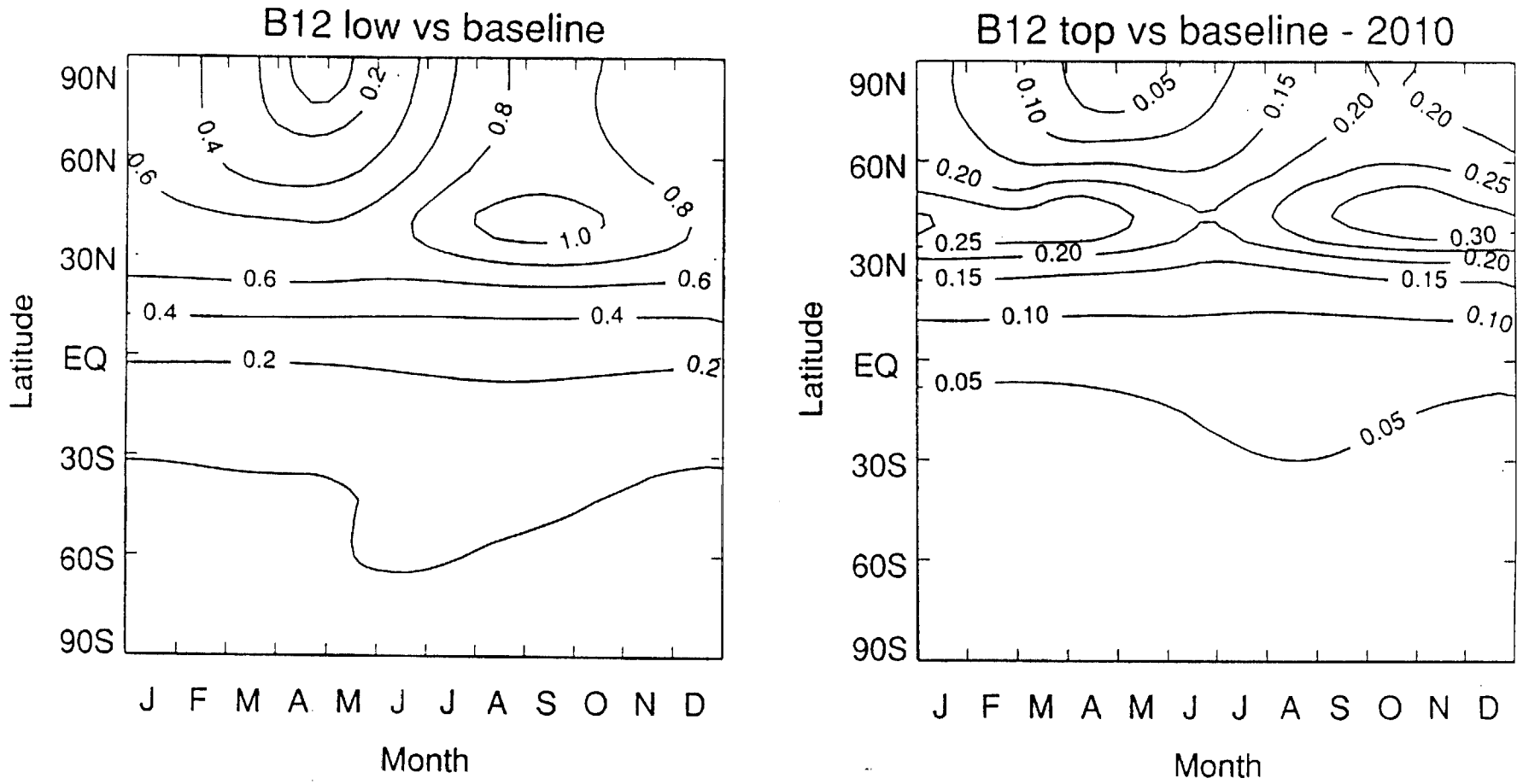

Figure 29. The calculated percent change in total ozone column from the baseline case for (a) scenario B12 emissions below 40000 ft and (b) B12 emissions at 55000 ft only, as a function of latitude and time of year.

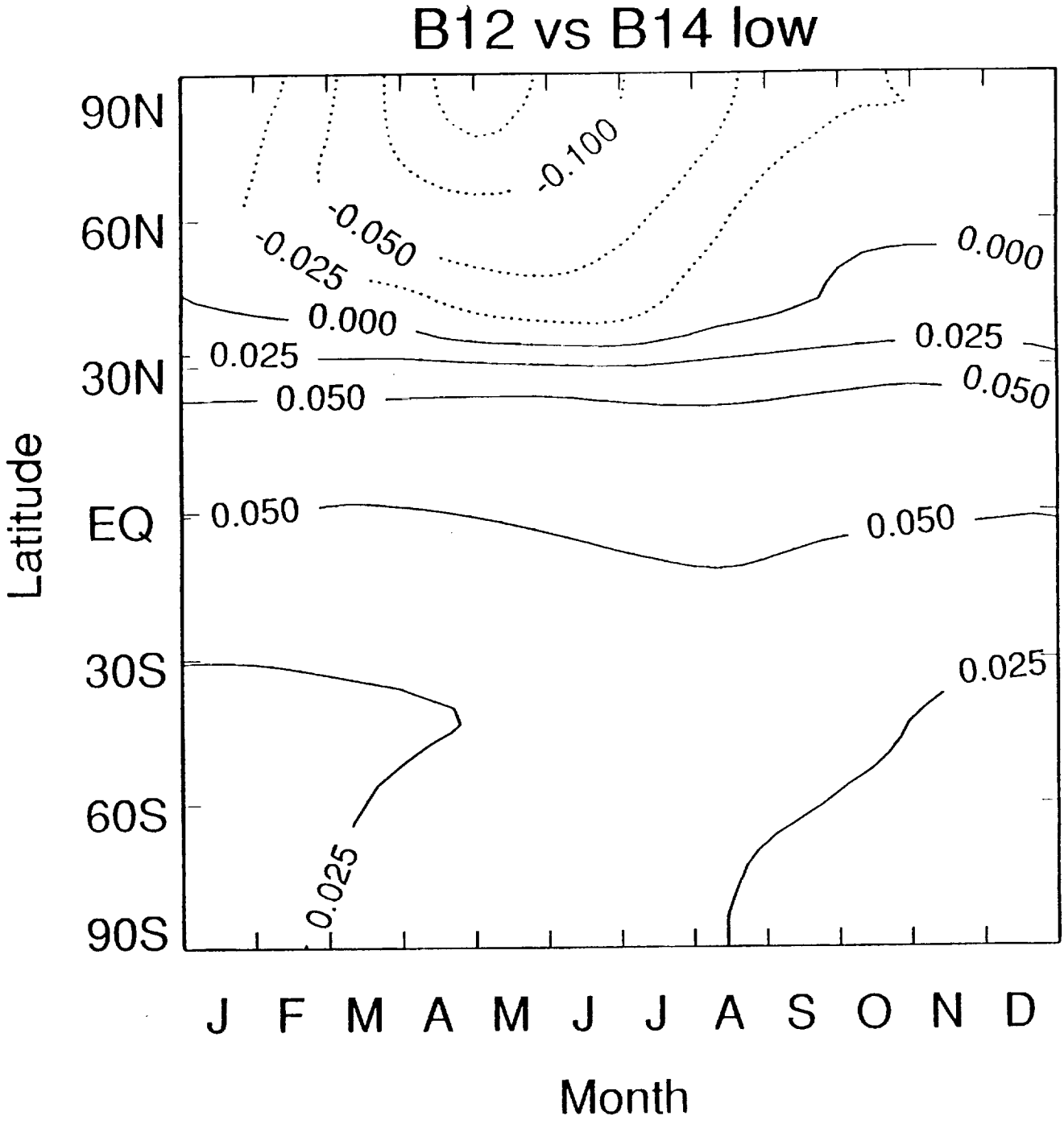

Figure 30. The calculated change in total ozone column for scenario B12 with emissions at all levels as a percentage of the ozone column with scenario B14 emissions below 40000 ft.

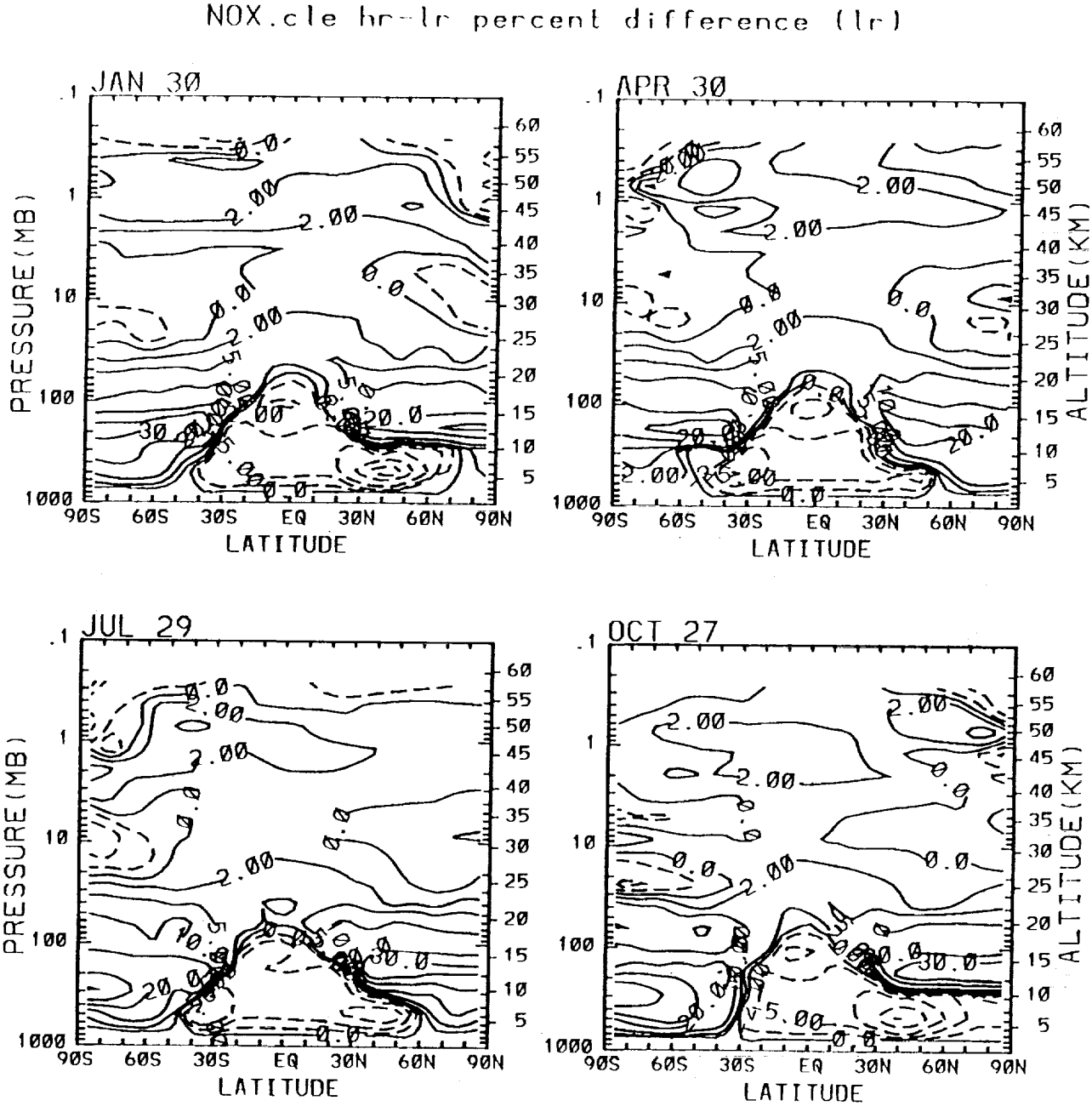

Figure 31. The percent difference in NOY mixing ratio for the clean atmosphere case from high-resolution model versus from coarse-resolution model for (a) January, (b) April (c) July, (d) October, as a function of latitude and altitude. Contours are 0, ± 2, ± 5, ± 10, ± 20, ± 30%.

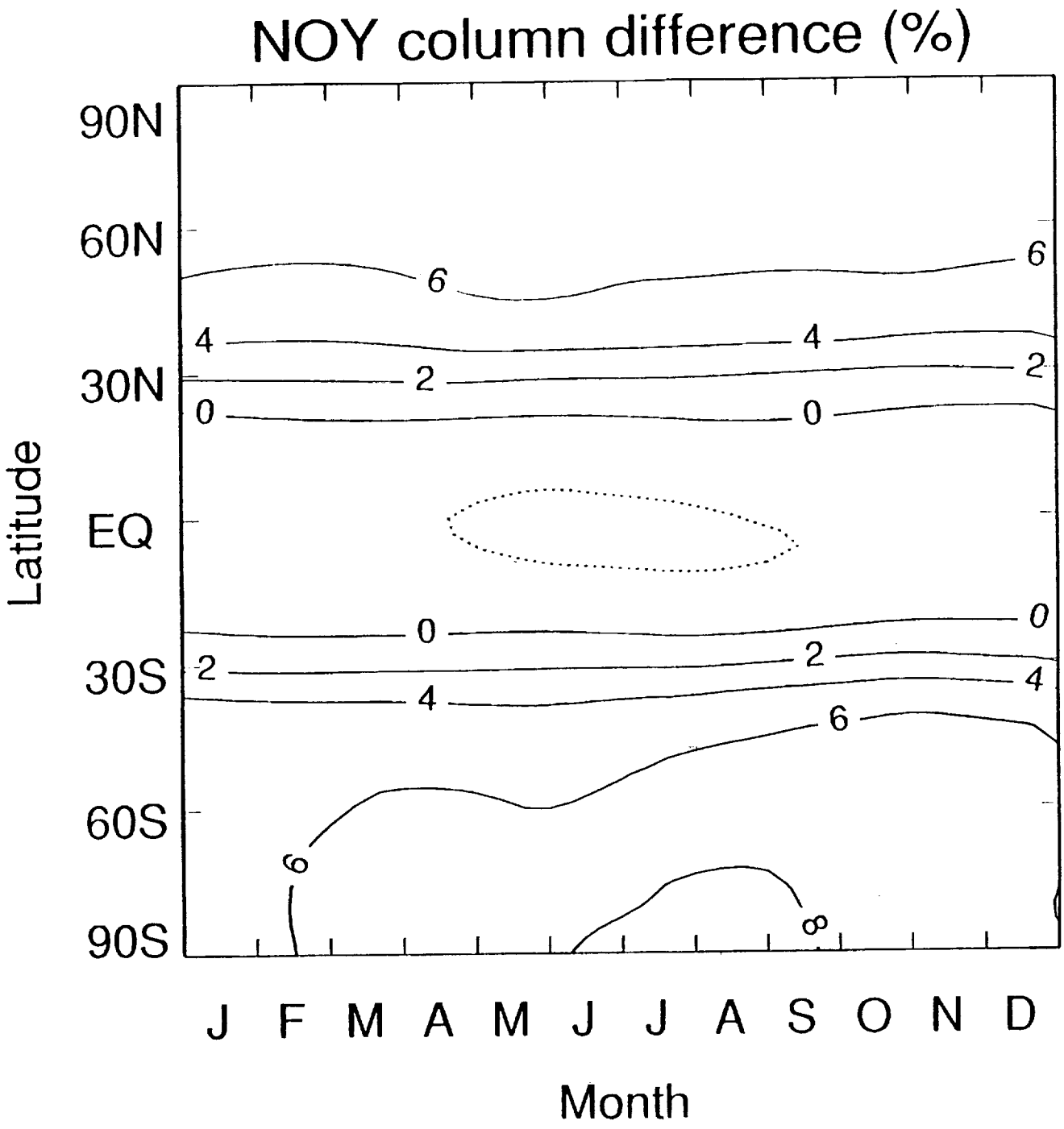

Figure 32. The percent difference in NOY column abundance for the clean atmosphere case from the high-resolution model versus from the coarse-resolution models as a function of latitude and time of year. Contours are -2, -1, 0, 2, 4, 6, 8 %.

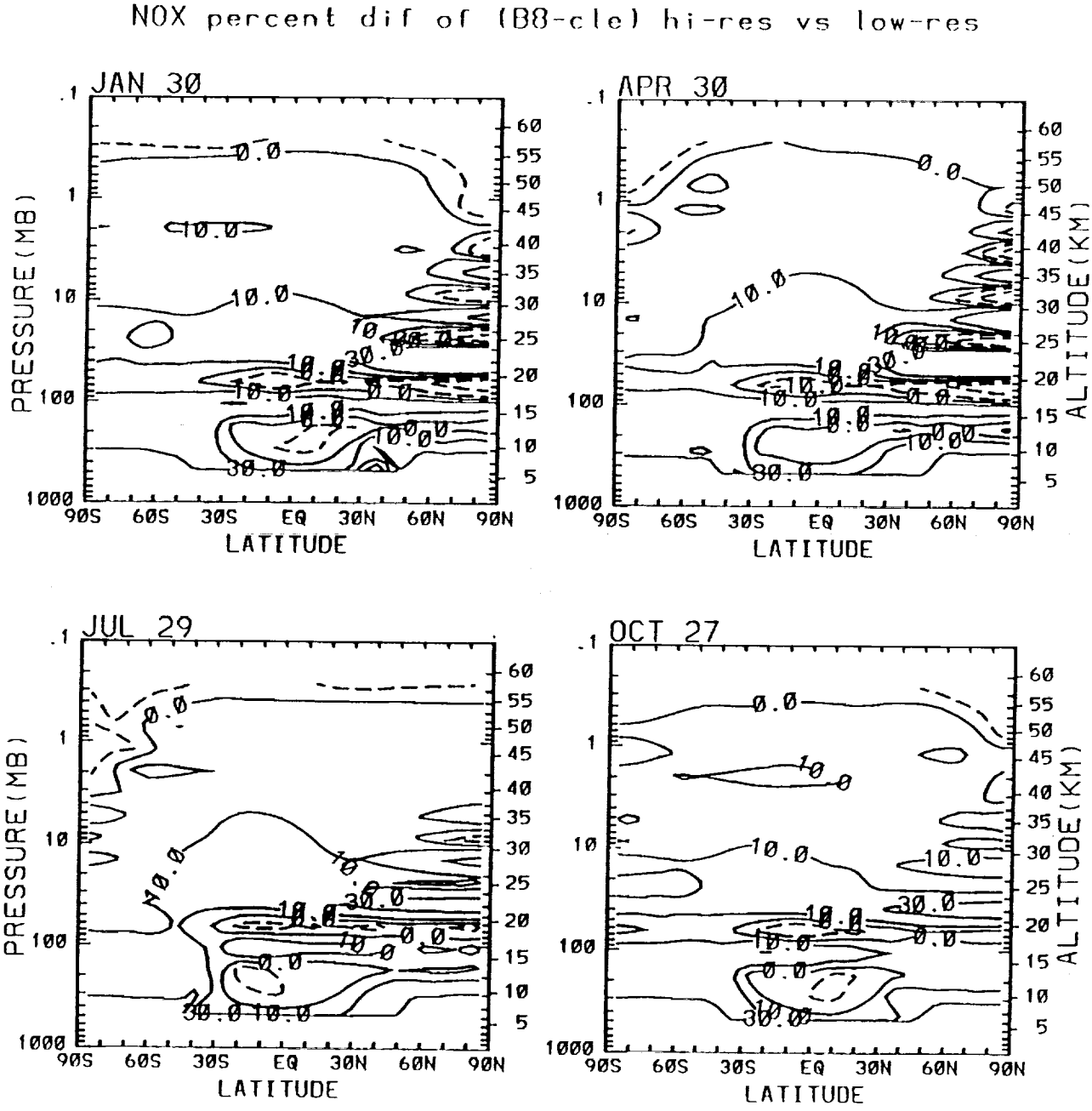

Figure 33. The percent difference in the NOY mixing ratio difference with scenario B8 emissions versus baseline for the high-resolution model versus the coarse resolution model, as a function of latitude and height for (a) Jan. (b), April, (c) July, and (d) October. See equation (11) in the text for a definition of the quantity plotted. Contours are 0, ± 10, ± 30%.

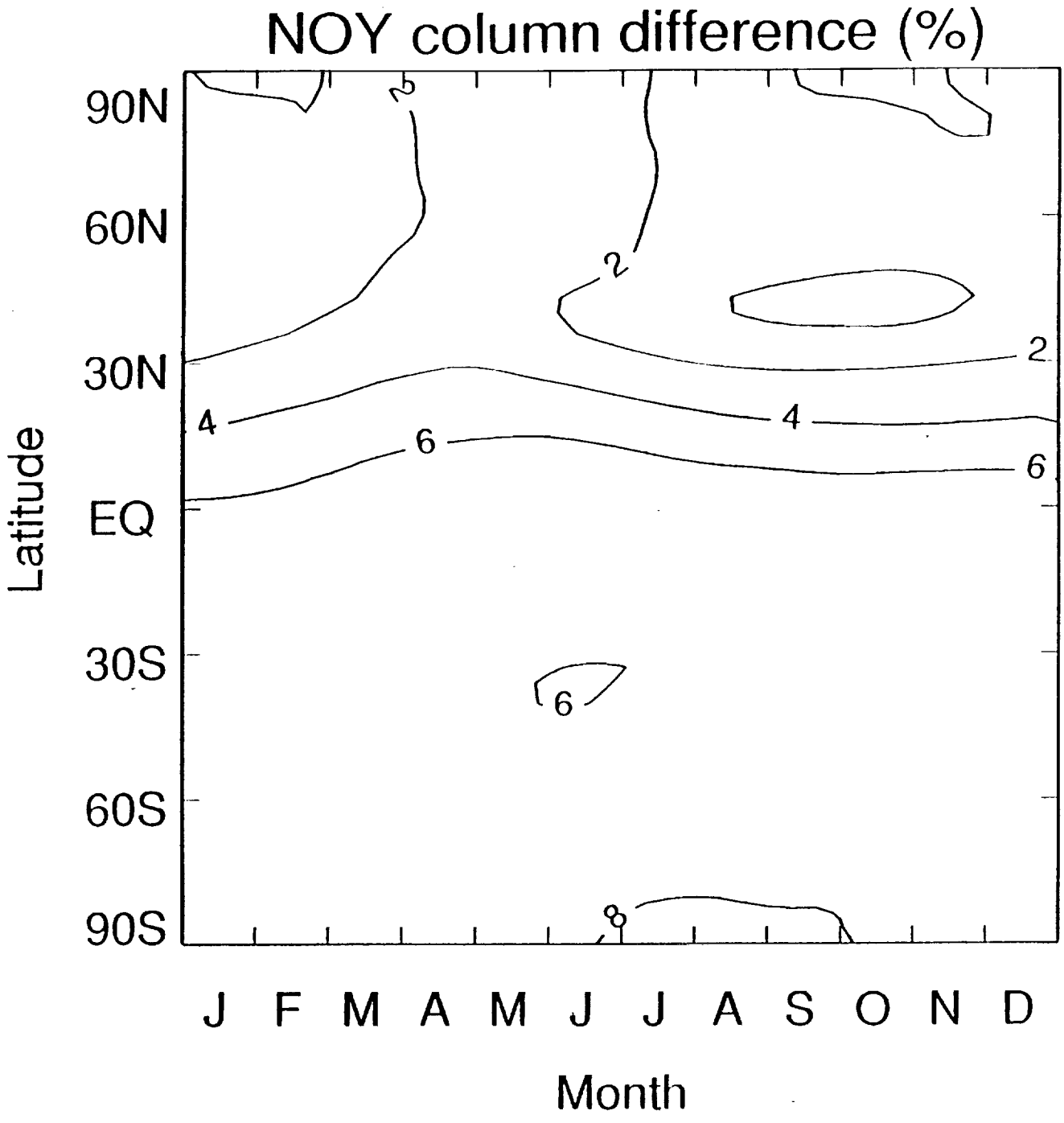

Figure 34. The percent difference in the change in NOY column abundance with scenario B8 emissions versus baseline for the high-resolution model versus the coarse-resolution model, as a function of latitude and time of year. Contours are 0, 2, 4, 6, 8 %.

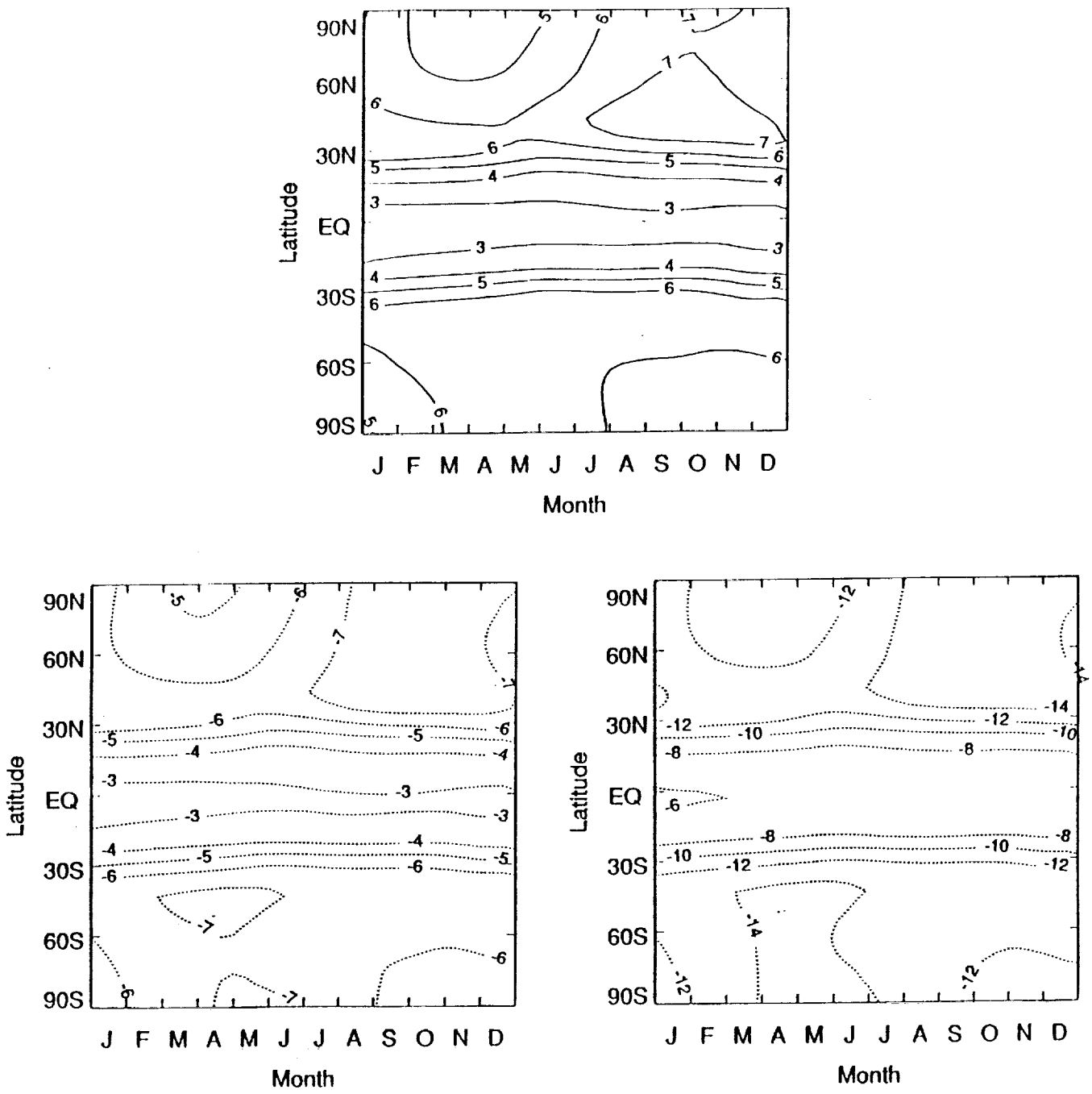

Figure 35. The percent difference in the NOY column abundance with the fine-resolution model for scenario A4 with (a) tropopause down 1 level, (b) tropopause up 1 level, and (c) tropopause up 2 levels versus scenario A4 with standard tropopause, as a function of latitude and time of year.

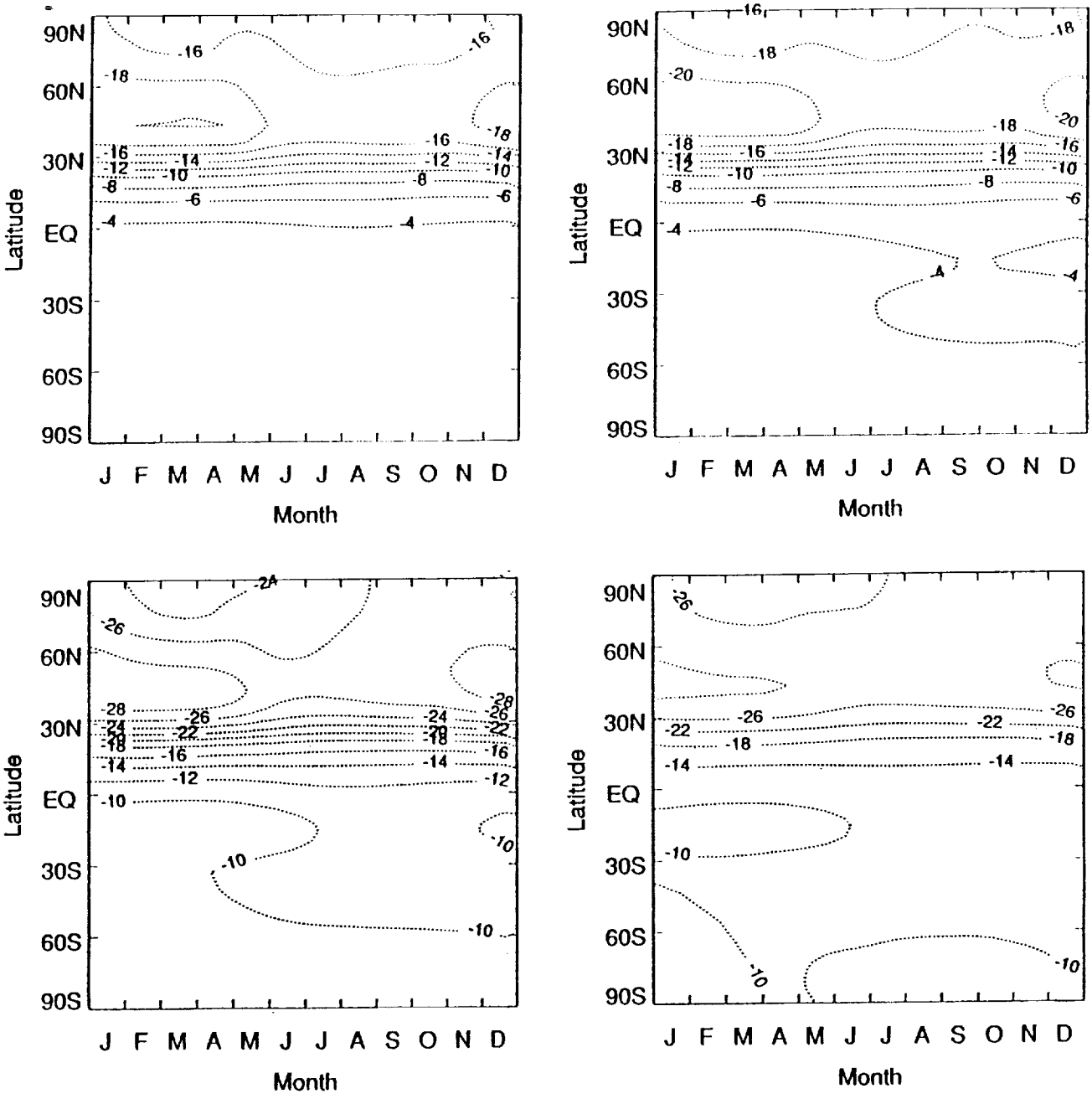

Figure 36. The percent difference in the NOY column abundance with the fine-resolution model using the scenario B8 emissions for the top altitude level only, with emissions (a) down 1 level, (b) down 2 levels, (c) down 3 levels, and (d) down 4 levels versus the standard B8 top level emissions.

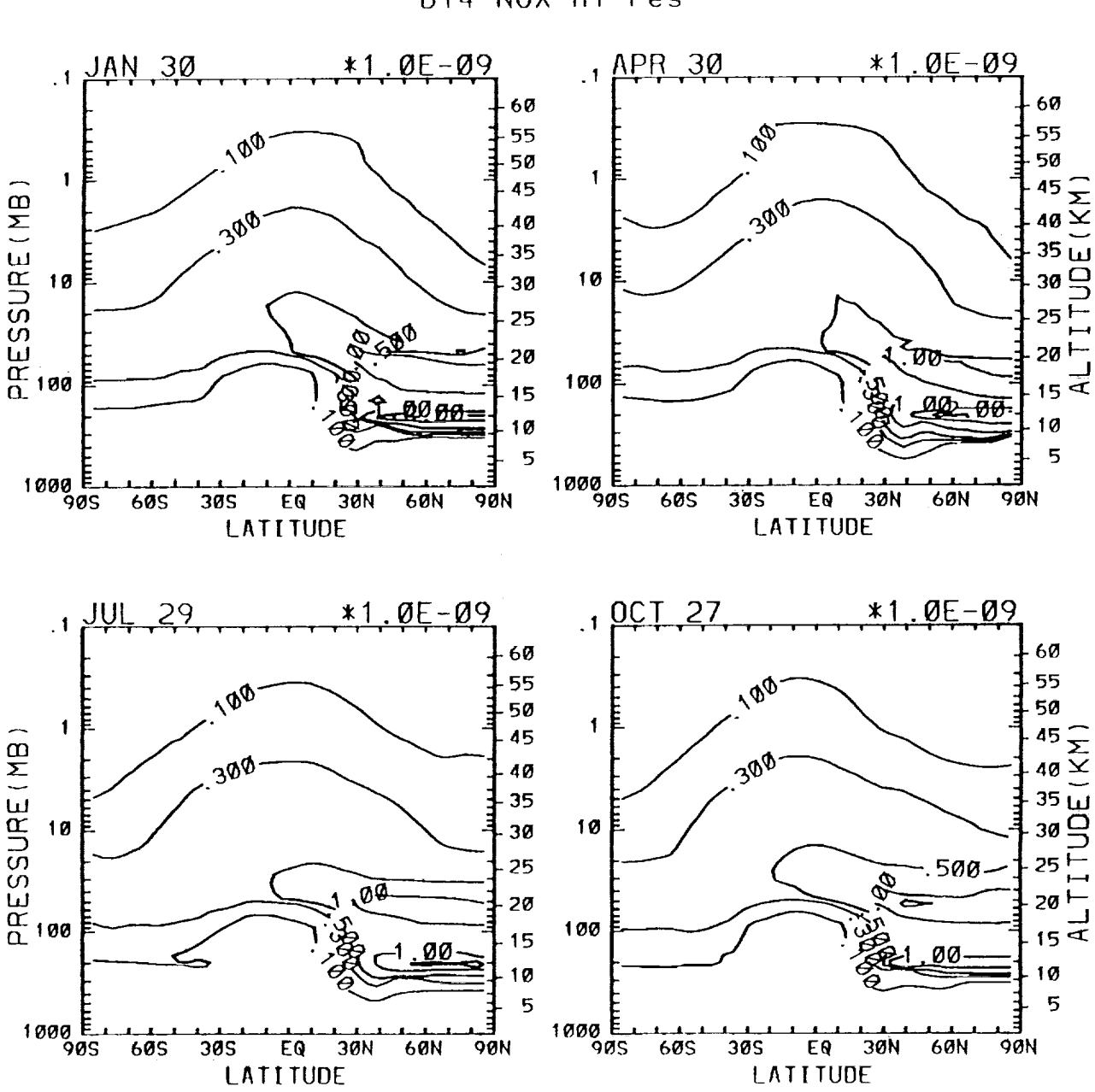

Figure 37. The change in NOY in ppbv calculated by the high-resolution model for scenario B14 emissions versus the baseline case as a function of latitude and altitude for (a) January, (b) April, (c) July, and (d) October. Contour levels are 0.6, 0.3, 0.5, 1, 2, 3, ppbv.

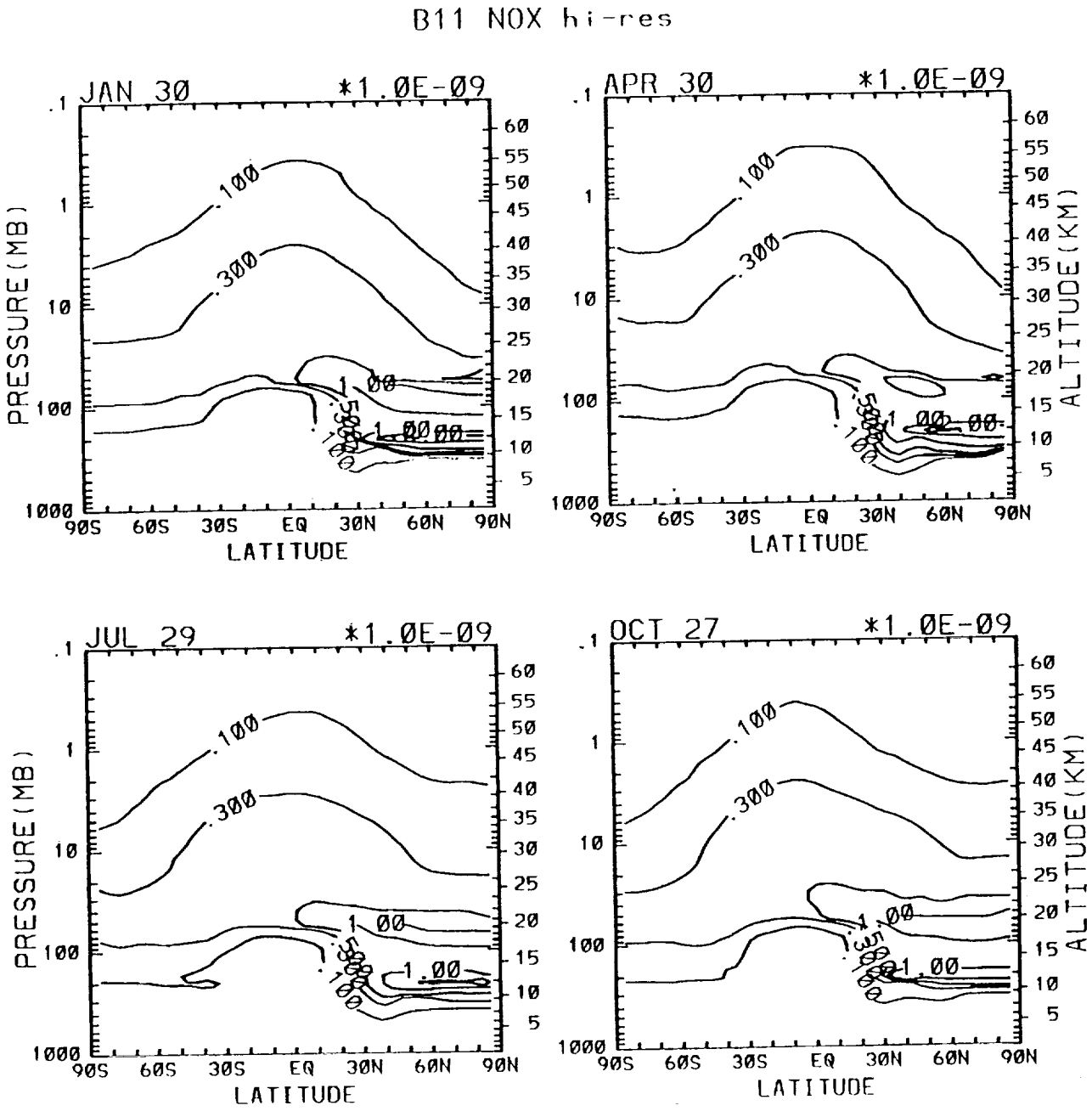

Figure 38. The change in NOY in ppbv calculated by the high-resolution model for scenario B11 emissions versus the baseline case as a function of latitude and altitude for (a) January, (b) April, (c) July, and (d) October. Contour levels are 0.1, 0.3, 0.5, 1, 2, 3, ppbv.

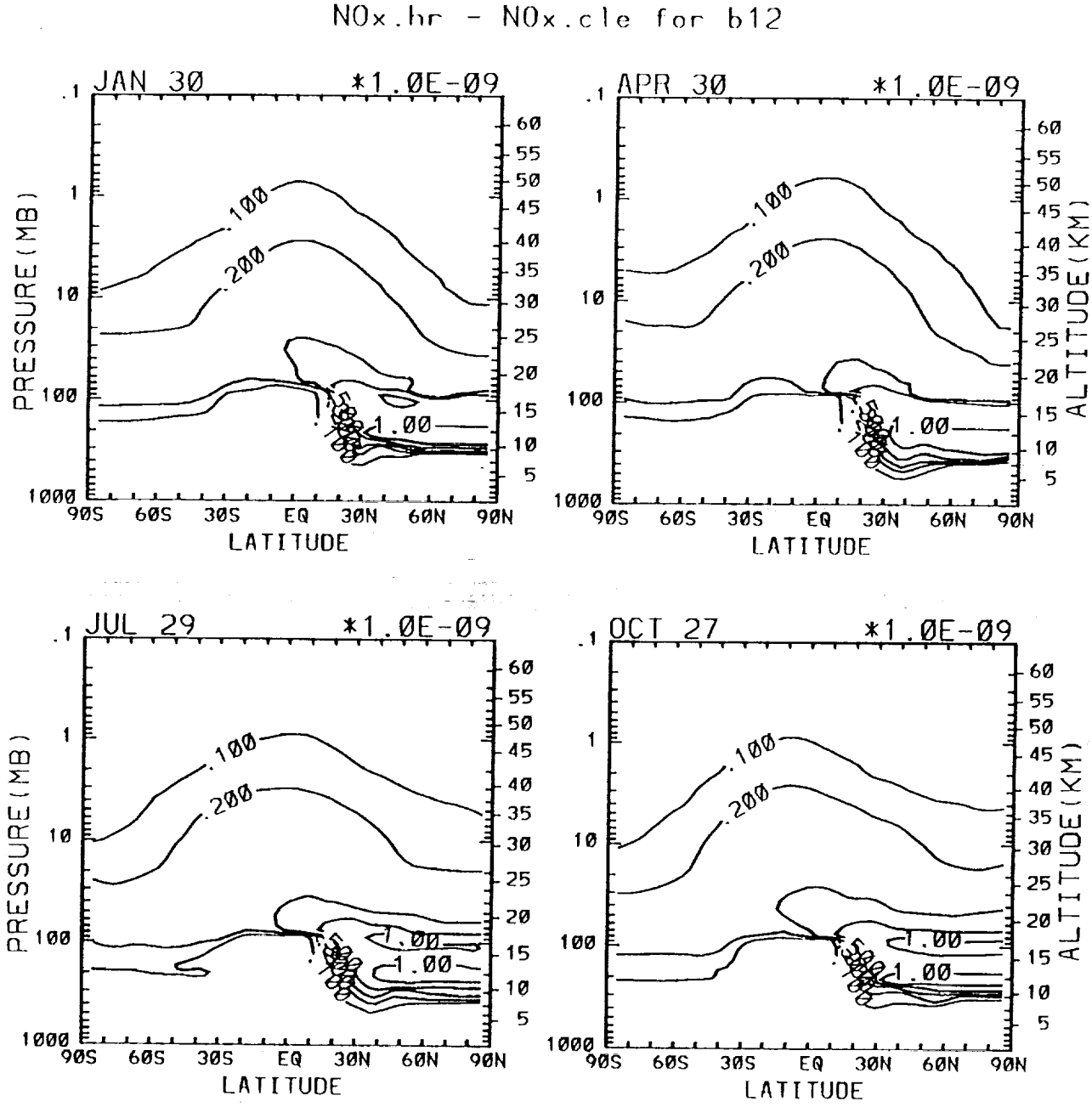

Figure 39. The change in NOY in ppbv calculated by the high-resolution model for scenario B12 emissions versus the baseline case as a function of latitude and altitude for (a) January, (b) April, (c) July, and (d) October. Contour levels are 0.1, 0.2, 0.3, 0.5, 1, 2 ppbv.

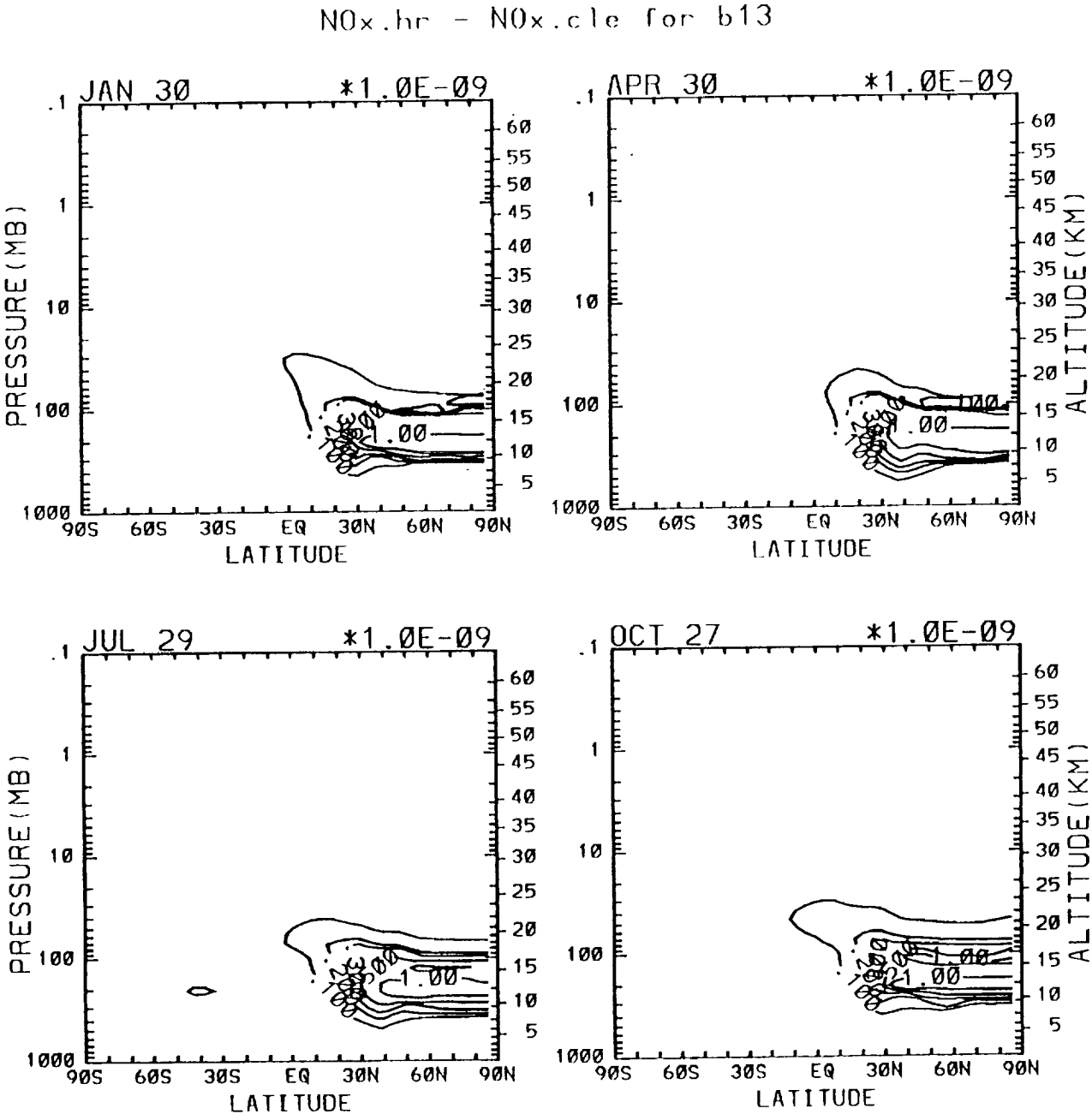

Figure 40. The change in NOY in ppbv calculated by the high-resolution model for scenario B13 emissions versus the baseline case as a function of latitude and altitude for (a) January, (b) April, (c) July, and (d) October. Contour levels are 0.1, 0.2, 0.3, 0.5, 1 ppbv.

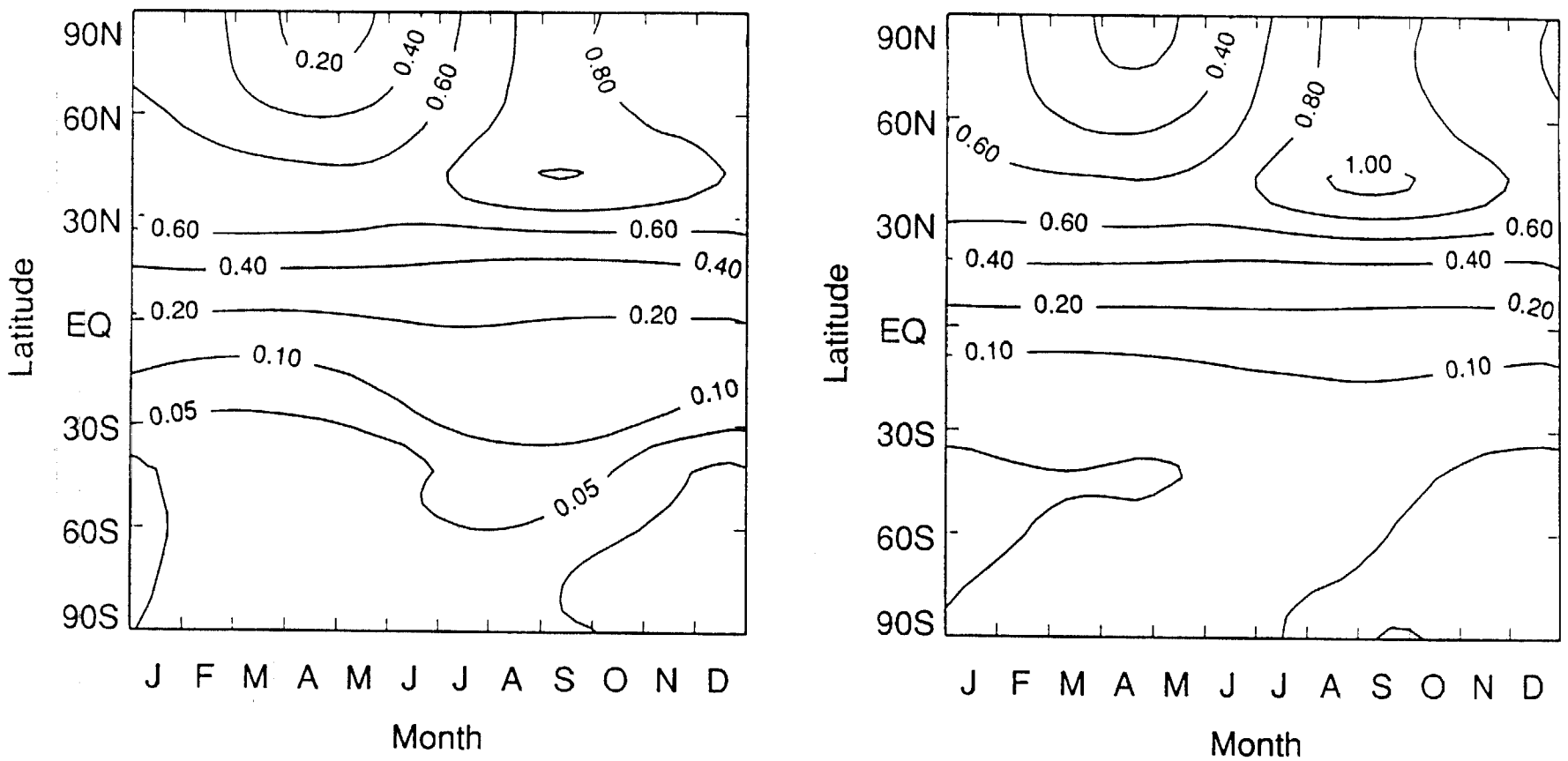

Figure 41. The calculated percent change in total ozone column for (a) scenario B12 and (b) scenario B13 versus the baseline case, using the NOY calculated by the high-resolution model within the coarse-resolution model, as a function, of latitude and time of year. Contours are 0, .05, .1, .2, .4, .6, .8, 1.0%.

NASA National Aeronautics and Space Administration

Report Documentation Page

1. Report No.	2. Government Accession No.	3. Recipient's Catalog No.
NASA CR-4346, Part II		

4. Title and Subtitle

Effects of Engine Emissions From High-Speed Civil Transport Aircraft: A Two-Dimensional Modeling Study, Part II

5. Report Date

March 1991

6. Performing Organization Code

7. Author(s)

Malcolm K. W. Ko, Debra K. Weisenstein, Nein Dak Sze, Run-Lie Shia, Jose M. Rodriguez, and Curtis Heisey

8. Performing Organization Report No.

10. Work Unit No.

505-69-61-04

9. Performing Organization Name and Address

ST Systems Corporation
Hampton, Virginia 23666

11. Contract or Grant No.

NAS1-18460

12. Sponsoring Agency Name and Address

NASA Langley Research Center
Hampton, Virginia 23665-5225

13. Type of Report and Period Covered

Contractor Report
July 1989-December 1989

14. Sponsoring Agency Code

15. Supplementary Notes

Malcolm K. W. Ko, Debra K. Weisenstein, Nein Dak Sze, Run-Lie Shia, Jose M. Rodriguez, and Curtis Heisey: Atmospheric & Environmental Research, Inc., Cambridge, MA.
Langley Technical Monitor: Linwood Callis
Prepared by Atmospheric & Environmental Research, Inc., Cambridge, Massachusetts, Under Subcontract 89-6209-E2176 to ST Systems Corporation.

16. Abstract

The AER two-dimensional chemistry-transport model is used to study the effect on stratospheric ozone (O_3) from operation of supersonic and subsonic aircraft in the 2010 atmosphere. Our results show that:

- the calculated O_3 response is smaller in the 2010 atmosphere compared to previous calculations performed in the 1980 atmosphere.
- with the emissions provided to us, the calculated decrease in O_3 column is less than 1%.
- the effect of model grid resolution on O_3 response is small provided that the physics is not modified.

17. Key Words (Suggested by Author(s))	18. Distribution Statement
Ozone Civil Transport High Speed	Unclassified - Unlimited Subject Category - 45

19. Security Classif. (of this report)	20. Security Classif. (of this page)	21. No. of pages	22. Price
Unclassified	Unclassified	68	A04

NASA FORM 1626 OCT 86

For sale by the National Technical Information Service, Springfield, Virginia 22161-2171

NASA-Langley, 1991